Effect of a deuterium gas puff on the edge plasma in NSTX

2014 Plasma Phys. Control. Fusion 56 095010

(http://iopscience.iop.org/0741-3335/56/9/095010)

IOP Publishing Plasma Physics and Controlled Fusion

Plasma Phys. Control. Fusion **56** (2014) 095010 (20pp) doi:10.1088/0741-3335/56/9/095010

Effect of a deuterium gas puff on the edge plasma in NSTX

S J Zweben[1], D P Stotler[1], R E Bell[1], W M Davis[1], S M Kaye[1], B P LeBlanc[1], R J Maqueda[2], E T Meier[3], T Munsat[4], Y Ren[1], S A Sabbagh[5], Y Sechrest[4], D R Smith[6] and V Soukhanovskii[3]

[1] Princeton Plasma Physics Laboratory, Princeton, NJ 08540, USA
[2] X Science LLC, Plainsboro, NJ 08543, USA
[3] Lawrence Livermore National Laboratory, Livermore, CA 94550, USA
[4] University of Colorado, Dept. of Physics, Boulder, CO 80309, USA
[5] Columbia University, Dept. of Applied Physics and Applied Math, New York, NY 10026, USA
[6] University of Wisconsin, Dept. of Engineering Physics, Madison, WI 53706, USA

E-mail: szweben@pppl.gov

Received 25 February 2014, revised 29 May 2014
Accepted for publication 13 June 2014
Published 8 July 2014

Abstract

This paper describes a detailed examination of the effects of a relatively small pulsed deuterium gas puff on the edge plasma and edge turbulence in NSTX. This gas puff caused little or no change in the line-averaged plasma density or total stored energy, or in the edge density and electron temperature up to the time of the peak of the gas puff. The radial profile of the Dα light emission and the edge turbulence within this gas puff did not vary significantly over its rise and fall, implying that these gas puffs did not significantly perturb the local edge plasma or edge turbulence. These measurements are compared with modeling by DEGAS 2, UEDGE, and with simplified estimates for the expected effects of this gas puff.

Keywords: tokamak, turbulence, NSTX

(Some figures may appear in colour only in the online journal)

1. Introduction

Almost all tokamak experiments use hydrogen or deuterium gas puffing to fuel the plasma and to increase the plasma density. These neutral molecular gases are puffed into the chamber through fast-acting valves at the vacuum vessel wall, and usually only a small fraction of this incoming gas enters the plasma edge and becomes ionized. The location and strength of these neutral gas sources is generally not well documented, and relatively little is understood about the effect of these gas puffs on the plasma.

The goal of this paper is to describe the effects of a deuterium gas puff on the edge plasma in NSTX, which is a low aspect ratio tokamak [1]. There are two different motivations for this study. The first is to determine whether this specific deuterium gas puff used for the NSTX gas puff imaging (GPI) diagnostic has any significant perturbing effects on the edge turbulence which it is designed to measure. The second motivation is to better understand the response of the plasma edge to the deuterium fueling puffs, using these GPI gas puffs as test cases.

The effect of a gas puff can be quite complex and difficult to predict from first principles, since it depends on the particle and energy transport mechanisms in the edge plasma, which are not well understood. In general, any edge particle source will increase the density where its ionization occurs, and the edge temperature nearby will decrease due to energy loss from ionization, radiation and charge exchange (CX) from the neutrals. The response of the plasma to these sources and sinks will depend on both the parallel and the cross-field transport.

The GPI diagnostic on NSTX measures the 2D structure and motion of edge turbulence by viewing the visible light emitted by a single short-pulse deuterium (or helium) gas puff introduced into the plasma edge [2–4]. Ideally, this gas puff should introduce as little gas as possible to minimize perturbations to the local edge plasma and/or to the edge turbulence. The earliest NSTX deuterium GPI results showed no changes in the turbulence characteristics versus time over a factor of $\sim\times5$ in the helium gas puff influx rate with a total gas puff of $\sim$1 Torr l (6.6×10^{19} D atoms or 3.6×10^{19} He atoms [2]). Later NSTX GPI results with similar gas puff levels

of helium or deuterium produced no significant change in either reflectometer or probe measurements of edge turbulence [3]. More recently the GPI deuterium gas influx rate has been increased to ~3–6 Torr l [4], partly due to the ×3 faster framing rate and smaller exposure time of the GPI camera, and partly due to a gradual radiation darkening of the fiber optic bundle carrying the images. The present paper reassesses these GPI gas puff effects at this higher gas influx rate.

The edge effects of gas puffs have been discussed in the context of several previous experiments. In the TJ-II stellarator [5], the edge Dα light was increased by deuterium gas puffing by a factor of up to 3.5 with no systematic changes in the edge turbulence. In PBX-M [5], helium gas puffing correlated with up to a factor of 2 increase in the relative edge turbulence level, but only when the edge electron temperature decreased by a factor of 2 due to the helium. In ASDEX Upgrade [6] and JET [7], deuterium puffs of ~(0.5–1.0) × 10^{22} atoms s^{-1} (similar to the present experiment) were recently used to improve the ICRH and LH coupling (respectively), but no measurements of edge turbulence were reported.

Gas puff effects were also studied in non-diverted hydrogen Ohmic discharges in the small ADITYA tokamak [8, 9]. Several effects on edge fluctuations and transport were observed, including a flattening of the edge floating potential profile, a decrease in edge density gradient, a reduction in edge floating potential fluctuations, and a ×2 increase in global confinement time [8]. These gas puffs also reduced the edge poloidal flow speed, and caused reversal in the toroidal flow speed due to the local edge particle source [9]. Gas puff effects in non-diverted hydrogen Ohmic discharges were also studied on the small STOR-M tokamak [10], where the line-averaged density was doubled by these gas puffs, but the loop voltage decreased, indicating an increase in the core electron temperature and global confinement. The scrape-off layer (SOL) density increased and electron temperature decreased ~1–3 ms after the puff, along with a reduction in the floating potential fluctuations, as in ADITYA [8].

The previous results most closely related to the present paper were obtained using GPI diagnostics on other tokamaks. Deuterium gas puff rates of ~10^{19}–10^{20} atoms s^{-1} were used in early GPI experiments on Alcator C-Mod [11], and no significant change in the fluctuations in a Langmuir probe at the same minor radius as the GPI gas cloud were observed. Helium gas puff rates up to ~10^{21} atoms s^{-1} were recently used for GPI in Alcator C-Mod [12], and estimates of the possible perturbing effects of these puffs were made, although edge plasma effects were not reported. Helium puffing was also used in the dual GPI diagnostic in the EAST tokamak [13] with an average puff rate (per GPI view) of ~2 × 10^{20} atoms s^{-1} over 250 ms, with an acceptable level of edge perturbation. In the TEXTOR tokamak a deuterium GPI system was operated with a low divergence gas nozzle [14], and measurements of edge density and temperature profiles in the edge and SOL showed no significant change with or without the puff up to gas influx rates ~4.6 × 10^{20} atoms s^{-1}, although a slight decrease in ion saturation current fluctuations at the outer midplane was observed by a Langmuir probe at the higher puff rates. The effect of the gas puff gas on the edge plasma in TEXTOR was not as strong as its effect on the global plasma density.

The response of the edge plasma to supersonic gas injection was also measured and modeled in Tore-Supra [15]. The amount of deuterium gas puffed was (1–5) × 10^{20} atoms in 2–4 ms, i.e. up to ~10^{23} atoms s^{-1}. Measurements made with Langmuir probes 2 cm outside the separatrix showed a large increase in the SOL plasma density and parallel Mach speed, and a factor of 2 decrease in the SOL electron temperature just after the gas puff. The local effects of strong deuterium gas fueling were also measured in TEXTOR during radiative improved (RI) modes operation [16]. The deuterium injection rate varied between 10^{20}–3 × 10^{21} atoms s^{-1}, and measurements were made of the deuterium atomic and molecular spectra in the gas cloud to infer the local electron temperature, which decreased significantly at the highest gas puff rates.

Other previous tokamak experiments have studied the interaction between gas puffing and the L–H transition. A strong gas puff was observed to rapidly increase the edge density and trigger an L–H transition in non-diverted Ohmic plasmas in the Tuman-3 tokamak [17]. In the low aspect ratio tokamaks MAST [18] and NSTX [19], it was found that high-field side (i.e. inner wall) gas fueling at a rate of ~3 × 10^{21} D atoms s^{-1} facilitates the L–H transition, compared with the usual low-field-side gas fueling.

Gas puffing experiments have been of more general interest for many years in the study of particle confinement in tokamaks; for example, in PLT [20], TEXT [21], TFTR [22], DIII-D [23], and recently in T-10 [24]. In most of these experiments the focus was on core particle transport, and there were relatively few measurements of the local effects of these gas puffs on the edge plasma, although a possible effect of the small gas puffs in T-10 on the edge temperature was noted in [24].

There have been several theoretical analyses of the effects of edge neutrals on poloidal $E \times B$ plasma flow in the context of L–H transition studies. Large deuterium gas puff rates of ~10^{22} atoms s^{-1} for ~0.5 s increased the neutral density and line-averaged plasma density significantly in DIII-D [25], and a correlation was found between the edge neutral density and the L–H power threshold. The effect of neutrals on various edge instabilities was analyzed in [26], and poloidally localized refueling was proposed as a method to control edge plasma rotation through the CX transfer of momentum [27]. The neoclassical theory of toroidal rotation in the presence of asymmetric gas puffing in the tokamak edge was discussed in [28]. Finally, recent simulations of L–H transitions also showed a sensitivity to the edge particle injection rate *via* changes in the edge temperature [29].

There has been an extensive series of theoretical analyses by Tokar *et al* of the local effects of deuterium or impurity gas puffs on the edge thermal stability and tokamak density limit [16, 30–33]. The most recent analysis [33] treats this problem by solving a non-stationary, two-dimensional (2D) heat conduction equation numerically, and includes a heat flux limit and the density response to edge cooling. 2D numerical modeling of the ionization of gas puffed atoms in the edge plasma has also been included in the comprehensive EDGE2D [34] and UEDGE codes [35], although the three-dimensional (3D) nature of a localized gas puff is beyond the scope of these codes.

Table 1. Shot list (no-puff shots in **bold**).

Shot	B (kG)	I (MA)	P (MW)	n^a	Gap[b]	Li[c]	Peak[d]	Puff[e]	Plasma type
138843	**4.4**	**0.8**	**3.9**	**6.5**	**10.2**	**104**	**0.613**	**0**	**NBI H-mode**
138844	4.4	0.8	3.9	6.5	10.1	112	0.613	5.7	NBI H-mode
138845	4.4	0.8	3.9	7.0	10.0	101	0.613	5.4	NBI H-mode
138846	4.4	0.8	3.9	7.1	10.1	104	0.613	5.7	NBI H-mode
139494	4.7	0.9	2.0	6.7	11.6	152	0.512	5.9	NBI H-mode
139495	**4.7**	**0.9**	**2.0**	**6.1**	**11.5**	**152**	**0.512**	**0**	**NBI H-mode**
139499	4.7	0.9	2.0	6.4	11.2	153	0.512	5.4	NBI H-mode
139500	4.7	0.9	2.0	6.3	11.4	152	0.512	5.5	NBI H-mode
139501	4.7	0.9	2.0	6.6	11.4	152	0.512	5.4	NBI H-mode
139044	4.9	1.0	6.0	5.7	10.3	0	0.412	5.4	NBI H-mode
139048	5.4	1.1	6.0	5.0	11.3	96	0.412	5.8	NBI H-mode
139286	4.9	0.8	3.0	3.7	10.9	293	0.314	5.7	NBI H-mode
139508	4.4	0.8	3.0	5.1	11.4	151	0.412	4.6	NBI H-mode
139509	4.4	0.8	3.0	4.5	11.8	141	0.412	4.3	NBI H-mode
139510	4.4	0.8	2.0	5.1	11.6	140	0.412	4.3	NBI H-mode
139443	5.4	1.1	0	2.9	9.9	81	0.287	4.8	Ohmic
141911	4.4	0.9	0	3.0	6.3	0	0.285	3.5	Ohmic
141912	4.4	0.9	0	3.0	6.5	0	0.285	3.5	Ohmic
141740	4.4	0.8	0	1.7	8.9	0	0.213	5.9	Ohmic
141741	4.0	0.7	0	1.9	9.3	0	0.213	5.7	Ohmic
141742	4.4	0.8	0	1.7	8.3	0	0.213	6.0	Ohmic
141754	3.6	0.8	0	2.0	8.6	0	0.213	5.7	Ohmic
141756	3.6	0.8	0	2.0	8.7	0	0.213	5.9	Ohmic
139441	5.4	1.1	2.0	2.5	10.1	80	0.287	5.4	NBI L-mode
139442	5.4	1.1	2.0	2.7	10.0	80	0.287	5.7	NBI L-mode
141984	4.4	0.9	1.1	2.5	2.8	0	0.224	3.7	RF L-mode
141985	4.4	0.9	1.1	2.5	3.1	0	0.224	3.5	RF L-mode

[a] Line-integrated density $\times 10^{15}$ cm^{-2} (divide by 120 to get line-averaged density).
[b] Distance in cm between separatrix and outer midplane RF antenna at 157.5 cm.
[c] Amount of lithium wall coating just before shot (mg).
[d] Time of the peak of the GPI puff (s).
[e] Total GPI gas puff in Torr l.

Finally, we mention other edge particle sources in tokamaks: supersonic gas nozzles in NSTX can inject up to $\sim 10^{22}$ atoms s^{-1} of deuterium to improve the fueling efficiency [36], and small deuterium pellets have been injected with (2–6) $\times 10^{21}$ atoms s^{-1} to control edge-localized modes (ELMs) in DIII-D [37]. Impurity gas puffing of nitrogen at a level of $\sim 10^{22}$ electrons s^{-1} has been used to increase edge radiation and reduce the SOL temperature e.g. in JET [38], and massive impurity gas injection has been used on DIII-D [39] and Alcator C-Mod [40] to terminate the discharge to mitigate disruptions.

The outline of this paper is as follows: section 2 describes the experimental results, section 3 describes the modeling and interpretation of these results, and section 4 includes a discussion these results.

2. Experimental results

Section 2.1 describes the plasma parameters and gas puff, section 2.2 describes the Thomson scattering measurements, and section 2.3 describes GPI profile data, which give the most direct measurement of the local effects of the GPI gas puff. Section 2.4 describes the GPI turbulence measurements, section 2.5 describes other diagnostic data, and section 2.6 describes the (absence of) effects of the puff on the L–H transition and ELMs.

2.1. Plasma parameters and deuterium gas puffs

Table 1 lists the plasma parameters for the 27 NSTX discharges from 2010 used for this paper. The plasma currents ranged from 0.7–1.1 MA, the toroidal fields from 3.6–5.4 kG, and the applied neutral beam injection (NBI) or radio frequency (RF) power from 0–6 MW. These are low aspect ratio plasmas with major radius $R \sim 85$ cm and minor radius $a \sim 65$ cm with a diverted, lower single-null shape with an elongation of $\sim$2.2 [1]. The typical shape and size of these plasmas is shown in figure 1(a).

The shots in table 1 were chosen to have constant global parameters within ± 100 ms of the peak of the GPI puff time in table 1, i.e. constant plasma current, B field, plasma shape, and NBI or RF power. Also these shots were selected to have no large transient events during the times of interest, e.g. no L–H transitions or large ELMs, and to have GPI data taken with the fastest possible rate for turbulence analysis (400 000 frames s^{-1}). Only the first two groups of shots in table 1 had 'no-puff' comparison shots with similar conditions (shown in bold in the table), although all shots include a 'pre-puff' period for comparison within the shot. All of these plasmas were all far from the Greenwald density limit, e.g. $n/n_G \sim 0.5$ for #138846 @ 0.6 s.

The deuterium gas puff hardware is the same as used previously for the GPI diagnostic on NSTX [2–4], as shown

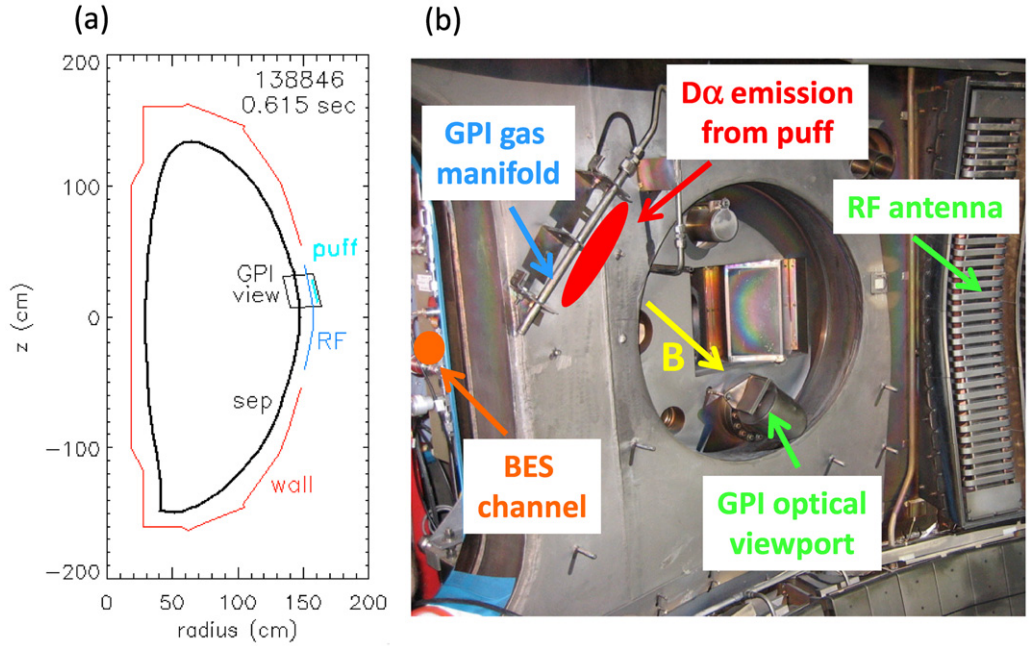

Figure 1. In (*a*) is a cross section of a typical plasma NSTX plasma in this experiment, and a picture of the GPI hardware inside the vessel is shown in (*b*). The GPI gas puff manifold is attached to the outer wall ∼20 cm above the midplane and about 2 cm behind the shadow of the nearby RF antenna limiter. The GPI Dα light emission is viewed over the 'GPI view' region shown in (*a*) using the optical viewport shown in (*b*). The location of the BES channel used for comparison with the GPI data is shown at the left in orange.

in figure 1(*b*). The GPI puff enters the plasma through a 30 cm long gas manifold located near the outer wall of the vessel and centered about 20 cm above the outer midplane, as previously described in [4]. The gas exits the manifold through 30 holes each of 1 mm diameter spaced 1 cm apart facing the plasma. The manifold holes were ∼2 cm radially behind the shadow of the RF antenna structure, which formed the outer midplane limiter in NSTX, and the radial distance of the magnetic separatrix from this limiter was typically ∼5–10 cm (see table 1). The manifold was oriented approximately perpendicular to the local edge B field direction, which was typically at an angle ∼40° with respect to horizontal in NSTX. The deuterium gas was stored in a room-temperature plenum, and a piezoelectric valve was triggered once per shot to fill the manifold and puff the gas into the plasma. The gas puffed into these plasmas ranged from ∼3–6 Torr l of deuterium per shot. No attempt was made to spatially collimate this gas puff or to create a supersonic gas nozzle.

Figure 2(*a*) shows the time dependence of the plasma current (top), NBI power, line-averaged electron density measured by Thomson scattering, and the total Dα light emission from the GPI puff for the first group of shots of table 1. Shot 138843 has no GPI puff, while the three successive shots have very similar GPI puffs of ∼5.4–5.7 Torr l. For these cases the GPI gas valve was pulsed at 0.580 s for 30 ms, the Dα light emission from this puff began to increase at 0.593 s, and the GPI Dα signal level peaked at 0.613 s at a level $\geqslant$20 times the background Dα before the GPI puff. About 20% of the time-integrated Dα light emission from the GPI puff occurred by the time of its peak, after which the Dα light decayed with an e-folding time of ∼50 ms due to draining of the gas manifold. About 80% of the total gas puff Dα light emission occurred by 67 ms after the peak of the Dα light emission.

Table 2 summarizes the gas puff parameters for a typical shot of figure 2(*a*). The total gas puff was 5.7 Torr l or 3.8×10^{20} deuterium atoms, with a peak neutral influx rate of $\sim 6.6 \times 10^{21}$ atoms s^{-1} and an average neutral influx rate over the first 100 ms of $\sim 3.2 \times 10^{21}$ atoms s^{-1}. The total number of neutrals puffed into the chamber by the time of the peak of the puff (0.613 s) is 7.6×10^{19} atoms, and by 67 ms after the peak this is 4× larger, i.e. $\sim 3 \times 10^{20}$ atoms. The total number of electrons inside the confined plasma just before the GPI puff was $N_{\rm tot} \sim 6 \times 10^{20}$ electrons, so the gas puff could potentially add ∼13% to the plasma electron content by the time of the peak of the gas puff, and ∼50% by 67 ms after the peak of the puff. However, only a small fraction (∼25%) of the neutrals coming from the manifold will be ionized in the main plasma, and these ions will quickly be lost by edge particle diffusion, so the expected global rise in density is $\leqslant$3% by the time of the peak of the puff. Particle balance estimates are discussed further in section 3.

The absolute level of Dα light emission from this puff was previously evaluated using the GPI imaging system, and was consistent to within ∼35% with the expected Dα light level for this gas puff, based on pressure gauge calibrations and DEGAS 2 simulations as described in [4]. Other deuterium gas sources for the discharge in figure 2(*a*) at the time of the GPI puff were $\sim(1.3\text{–}1.9) \times 10^{21}$ D s^{-1} from the center stack gas injector (slowly decaying from a puff started earlier in the shot), $\sim 4 \times 10^{20}$ D s^{-1} from NBI (according to TRANSP), $\sim 1.2 \times 10^{22}$ D s^{-1} recycled from the outer divertor target and $\sim 1.4 \times 10^{22}$ D s^{-1} recycled from the inner divertor target (according to UEDGE). Thus the peak GPI gas puff rate was $\leqslant$25% of the total neutral deuterium influx rate at that time, most of which came from recycling in the divertor region.

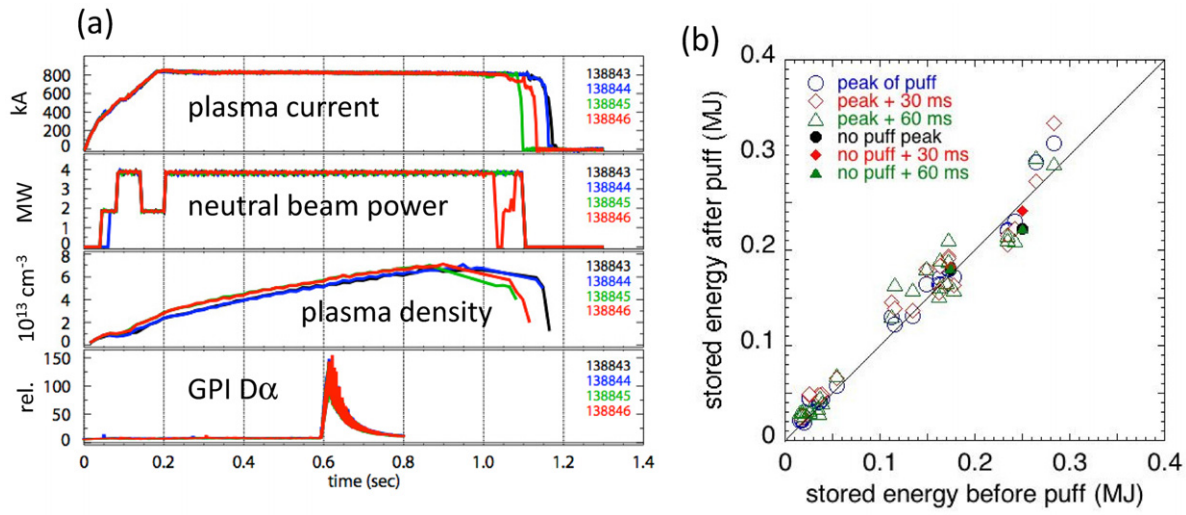

Figure 2. (*a*) shows the time dependence of the plasma current, neutral beam (NBI) power, line-averaged electron density, and the GPI Dα light emission for the first group of shots of table 1. Shot 138843 had no GPI puff, while the three successive shots have similar GPI puffs. There is no visible effect of the GPI puff on the time evolution of the line-averaged electron density in these cases. (*b*) shows the total stored energy before versus after the GPI puff for all the shots of table 1, again showing no systematic effect of the puff. Points in solid colors in (*b*) are with no GPI puff.

Table 2. Deuterium gas puff parameters (#138846).

	By the time of peak of puff (0.613 s)	By 67 ms after the peak (0.680 s)	All gas puff duration (0.593–0.800 s)
Neutrals puffed	7.6×10^{19} D atoms	3.0×10^{20} D atoms	3.8×10^{20} D atoms
Neutral influx rate	6.6×10^{21} D atoms s^{-1}	3.2×10^{21} D atoms s^{-1}	1.8×10^{21} D atoms s^{-1}
Total plasma electron content	$\sim 6 \times 10^{20}$ electrons	$\sim 6.4 \times 10^{20}$ electrons	—

There is no visible effect of these GPI gas puffs on the time evolution of the line-averaged electron density in NSTX, as illustrated in figure 2(*a*). This is in part because the density is continuously rising versus time even without the puff, since there is not enough wall pumping to maintain a steady-state density [41]. Figure 2(*b*) shows the total plasma stored energy before versus after the GPI puff for all the shots in the database of table 1, based on the energy inferred from the EFIT magnetic equilibria. The horizontal axis shows the stored energy just before (by ~10 msec) the start of the GPI puff for each shot, and the vertical axis shows the stored energy at the peak of the GPI puff and 30 and 60 ms later. The solid points show the 'no-puff' comparison shots for the first two groups in table 1, and the black line is drawn at unity slope. The ratio of the stored energy during the GPI puff to just before the GPI puff was 1.1 ± 0.2 at the peak of the puff, 1.2 ± 0.3 at 30 ms after the peak, and 1.2 ± 0.3 at 60 ms after the peak. Thus the GPI gas puff does not significantly change the total stored energy, and also does not affect the magnetic separatrix location or the radiated power, as discussed in section 2.5.

2.2. Thomson scattering data

The Thomson scattering diagnostic measures the electron density and temperature profiles on the NSTX midplane ~150° toroidally away from the GPI puff, and also far from the magnetic field lines going through the puff. These measurement channels have a radial separation of ~2 cm, a time separation of 16.6 ms, with error bars based on the photon statistics.

Figure 3 shows a comparison of the full Thomson profile contours for two of the shots of figure 2(*a*), one without a puff in figure 3(*a*) and with a GPI puff in figure 3(*b*), along with the line-integrated density, the maximum (i.e. central) electron temperature, and GPI Dα signals below. The magnetic axis locations in the contour plots are shown as the white dotted–dashed lines, and the separatrix locations are shown as the yellow dashed lines. The density is not significantly affected by the gas puff, but there appears to be some decrease in the edge temperature after the peak of the puff. The line-integrated density and central electron temperature are not significantly different between these puff and no-puff shots.

The variation in edge parameters during the GPI puff is illustrated more clearly in figures 4 and 5. These figures show the time and spatial dependence of the Thomson edge T_e and n_e data for the four shots of figure 2(*a*), with one shot without a gas puff (black) and the other three with a gas puff (green, red and blue). The separatrix position is constant within 0.2 cm from shot-to-shot, as listed in table 1. All of these shots are H-mode plasmas.

Figure 4 shows the time dependence of the Thomson T_e and n_e data for four spatial locations. There is little or no systematic change in either T_e or n_e with respect to the 'no-puff' comparison shot up to the time of the peak of the GPI puff, indicated by the vertical black lines. However, in the shots with a gas puff there was a ~20–30 ± 10% decrease in T_e by ~50–100 ms after the peak of the GPI puff at radii $\rho = -7.4$,

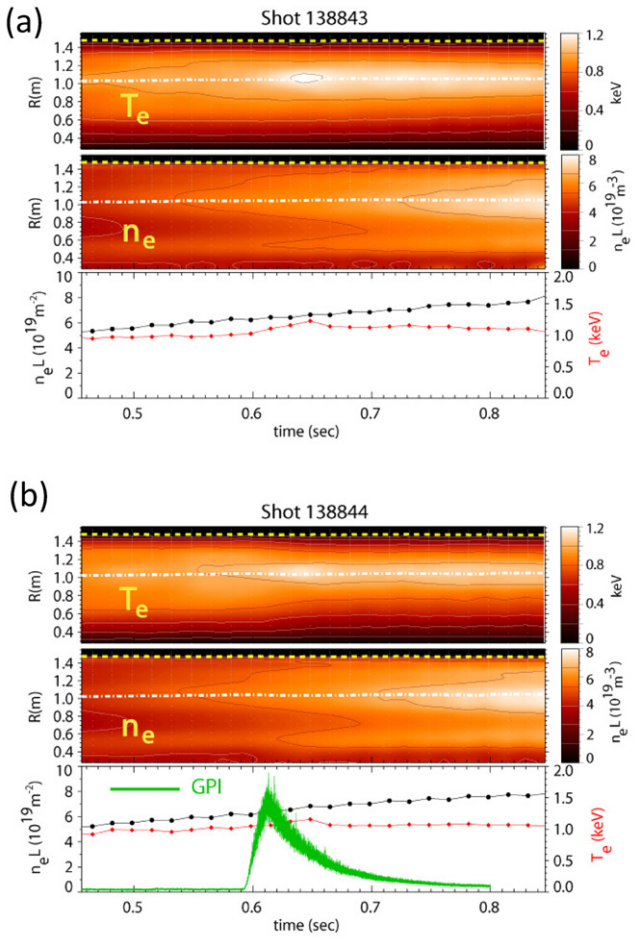

Figure 3. Comparison of the Thomson scattering profiles for shots without a GPI gas puff (*a*) and with a GPI gas puff (*b*) as a function of time, along with the line-integrated density, maximum (i.e. central) electron temperature, and GPI Dα signals below. The magnetic axis locations in the contour plots are shown as the white dotted–dashed lines, and the separatrix locations are shown as the yellow dashed lines. The density profile is not significantly affected by the gas puff, but there appears to be some change in the edge temperature after the peak of the puff.

−5.4 and −3.8 cm inside the separatrix in figures 4(*a*)–(*c*), when compared with the 'no-puff' shot. There were also ∼10–15% increases in n_e at 5.3 and 3.8 cm inside the separatrix by ∼50 ms after the peak of the puff, but little or no density increases at 7.4 cm inside the separatrix. The measurements at 1.4 cm inside the separatrix in figure 4(*d*) are dominated by random-looking fluctuations. The second group of shots in table 1 shows qualitatively similar trends to those in figures 4, but at slightly lower edge temperatures due to the lower NBI power.

Figure 5 shows the radial profiles of T_e and n_e for the same shots as for figure 4 for four different times, i.e. 31 ms before and 2, 35 and 69 ms after the peak of the GPI puff. The horizontal axis is the distance from the outer midplane separatrix, and the H-mode 'pedestal' in density occurs ∼2–4 cm inside the separatrix. Also shown at the bottom of the T_e plots are the radial profiles of the GPI Dα light emission for these times (black dots), mapped along flux surfaces to the outer midplane where the Thomson data is taken. The profiles in figure 5(*a*) at 31 ms before the peak of the GPI puff are similar for all four shots. The profiles in figure 5(*b*) taken ∼2 ms after the peak of the GPI puff show little or no systematic change, but the profiles below at 35 and 69 ms after the peak of the GPI puff in figures 5(*c*) and (*d*) show a clear decreases in T_e from ∼4–10 cm inside the separatrix, which is radially well inside the peak of the GPI Dα signal. The data in the SOL does not show consistent trends within the error bars.

To help clarify these trends, figure 6 shows all the T_e and n_e data in figure 5 for the first two groups of shots in table 1, but sorted by time with respect to the peak time of the gas puff. The electron temperatures are plotted in figure 6(*a*) and (on log scale) in figure 6(*b*), and the densities are plotted in figure 6(*c*) and (in log scale) in figure 6(*d*). The plots in log scale at the right are intended to show the low temperature and density edge points more clearly than in the linear plots at the left. The points from the shots with no GPI gas puff are marked in solid colors. For each plot the horizontal axis shows the T_e or n_e just before the puff starts (i.e. ∼31 ms before the peak of the gas puff), and the vertical axis shows the values at three successive times, each separated by 33 ms. Linear fits to the data are shown by the lines in figures 6(*a*) and (*c*).

The T_e points at the peak of the GPI puff in open blue circles in figure 6(*a*) are very near to the unity line shown in black, with a linear fit as shown with a slope of 0.93, while at 33 ms and 67 ms after the peak of the GPI puff the linear fits have slopes of 0.81 and 0.74, respectively. The shots with the largest effects in T_e at 67 ms after the peak are from 138844–139846 (group 1 of table 1), as indicated by arrows to the upper green triangles in figure 6(*a*), and shots at this time labeled 139494–139501 (group 2 of table 1) are at lower T_e and lower NBI power. The decreases in T_e at later times are mainly in the region where $T_e \geqslant 0.2$ keV, with little or no systematic change in T_e for the edge where $T_e \leqslant 0.1$ keV, as shown in the log plot in figure 6(*b*). Thus these temperature decreases are localized radially inside the peak of the ionization region of the gas puff. There is also a small systematic increase in density at 33 and 67 ms after the peak of the puff at $n_e \geqslant 3 \times 10^{13}$ cm^{-3}, some of which is due to the usual ∼10% per 100 ms increase in average density versus time in NSTX (see figure 2(*a*)). In the edge region where $n_e \leqslant 3 \times 10^{13}$ cm^{-3} there is little or no systematic density change at 33 and 66 ms after the peak of the puff, as shown in the log plot in figure 6(*d*).

The slopes of the linear fits in figure 6 are shown in the first entries in table 3. In addition, the average ratio of electron temperature or density during the puff to that just before the puff is shown by the second entry in this table. For example, the fit to the T_e data at the peak of the gas puff in figure 6(*a*) has a slope of 0.93, and the average ratio of T_e at the peak of the puff to before the puff was 1.10 for these points. The difference between these two numbers is due to different weighting of the points at low and high temperature. Thus there is on average ⩽10% change in T_e by the time of the peak of the gas puff in this data.

Figure 7 shows the T_e and n_e data for the 3rd, 4th and 5th groups of shots of table 1 (those without any no-puff comparison shots), plotted in the same way as for figure 6.

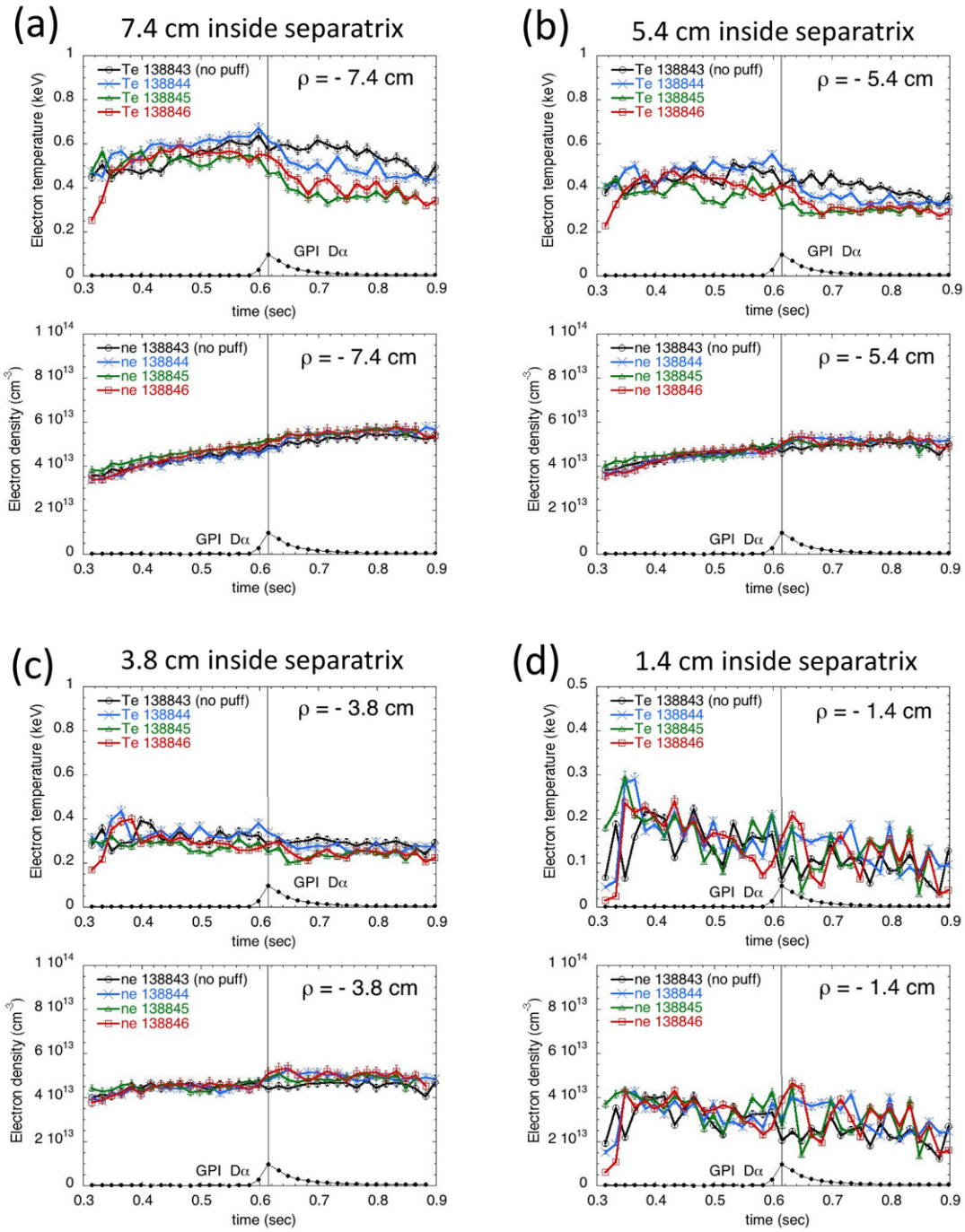

Figure 4. Time dependence of T_e and n_e measured by Thomson scattering over ±0.3 s around the GPI puff time for the same shots in figure 2(*a*), one without (138843) and three with a puff. (*a*)–(*d*) shows the results for radii of $\rho = -7.4$, -5.4, -3.8 and -1.4 cm inside the separatrix. The total Dα light versus time from the GPI puff is shown by the black dots at the bottom of each plot. The edge T_e decreases ∼50 ms after the puff starts for regions more than ∼4 cm inside the separatrix, and the n_e increases slightly over ∼50 ms after the puff starts for regions near ∼5 cm inside the separatrix.

These data are sorted in terms of H-mode shots in figures 7(*a*) and (*d*), L-mode shots in figures 7(*b*) and (*e*), and Ohmic shots in figures 7(*c*) and (*f*), and plotted for three times during the puff. The L-mode and Ohmic shots are generally shorter and less stationary in time than the H-mode shots. The most significant trend in figure 7 is a lower T_e after the puff in the L-mode and Ohmic cases, but there is a relatively large scatter around all the linear fits, partly due to small uncontrolled motion of the separatrix, and partly due to large turbulent fluctuations in the edge n_e and T_e, as noted previously [3]. Another cause of these variations in the H-mode cases is the sharp edge pedestal gradients, which can create relatively large local changes at a fixed radius even for $\leqslant$1 cm shifts in the location of the separatrix.

Each group of points in figure 7 is fit by a linear curve, and the slopes of these fits are summarized in the first entries in table 3, along with similar fits to the shots from figure 6. For the H-mode cases, which are near to steady-state conditions

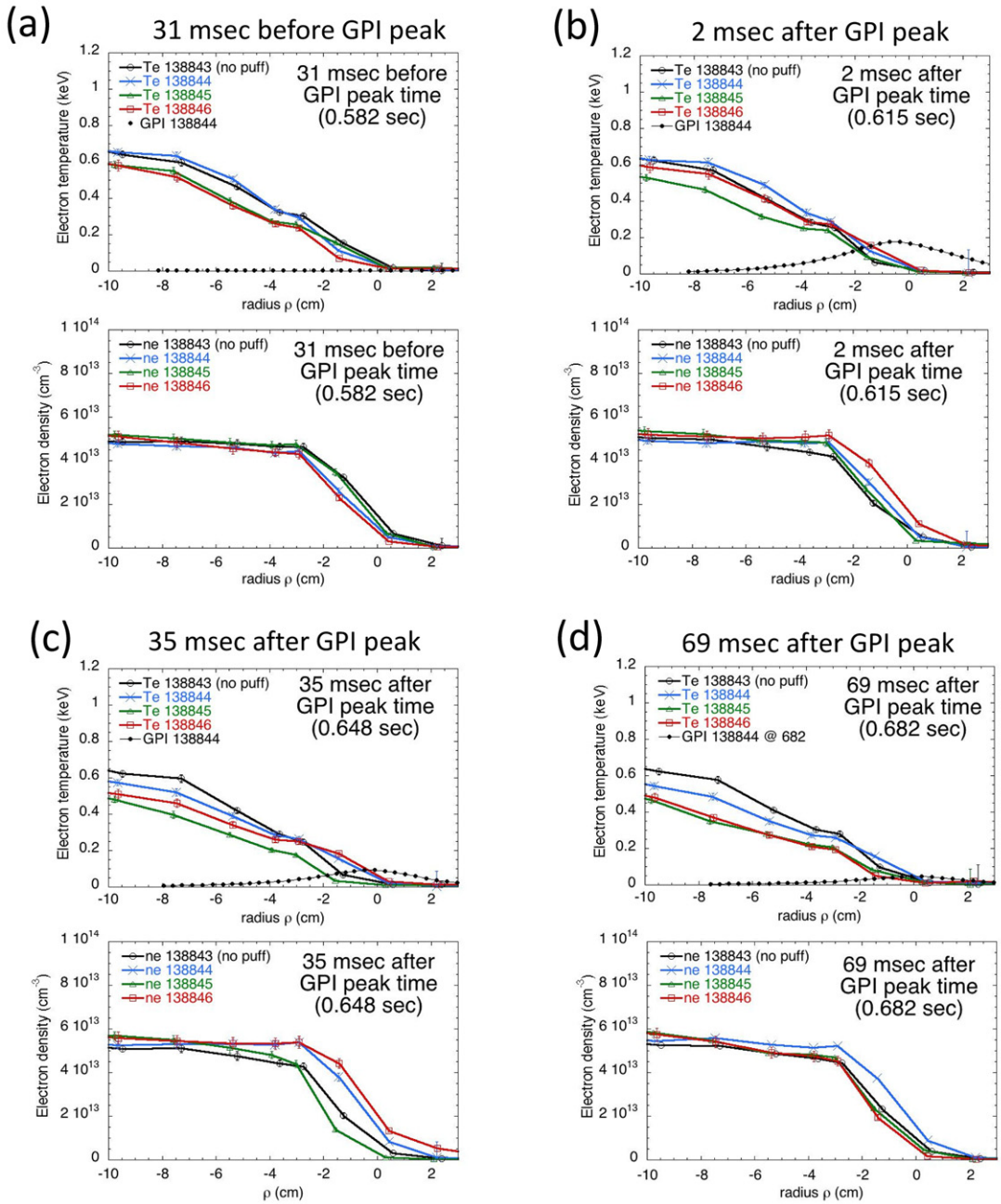

Figure 5. Radial dependence of T_e and n_e measured by Thomson scattering for four different times for the same four shots as figure 4, including one shot with no GPI puff (138843). The horizontal axis is the distance from the outer midplane separatrix for each shot. (*a*)–(*d*) are for times with respect to the peak of the puff of −31, +2, +35 and +69 ms. (*c*) and (*d*) show that T_e decreases significantly 36 and 70 ms after the peak of the GPI puff, but only at radii more than ∼4 cm inside the separatrix. The shot-to-shot differences in the radial location of the data points are due to the slightly different separatrix locations, as listed in table 1. The radial profiles of the gas puff Dα emission are shown by the black dots in the T_e plots.

without any puff, these slopes are all within 10% of unity for both density and electron temperature at the time of the peak of the GPI puff. All of the other cases have fitted slopes within ±20% of 1.0 at the peak of the puff, and almost all are within 25% of 1.0 at later times. The same data was also analyzed by finding the average ratio of electron temperature or density during the puff to that just before the puff, as shown by the second entry in each box in this data table. All of these after/before ratios are within 20% of unity at the peak of the gas puff. The Ohmic cases show the largest reduction of the edge electron temperature late in time, but this may be due to natural time-varying plasma conditions and not to the GPI puff itself.

2.3. GPI profile data

The only direct measurement of the local effects of the GPI gas puff in this experiment is from the radial profile of the GPI Dα emission itself, since this profile depends on the local plasma density and temperature profiles [4]. In this section we describe these profiles for nearly stationary H-mode shots like those in figure 2(*a*).

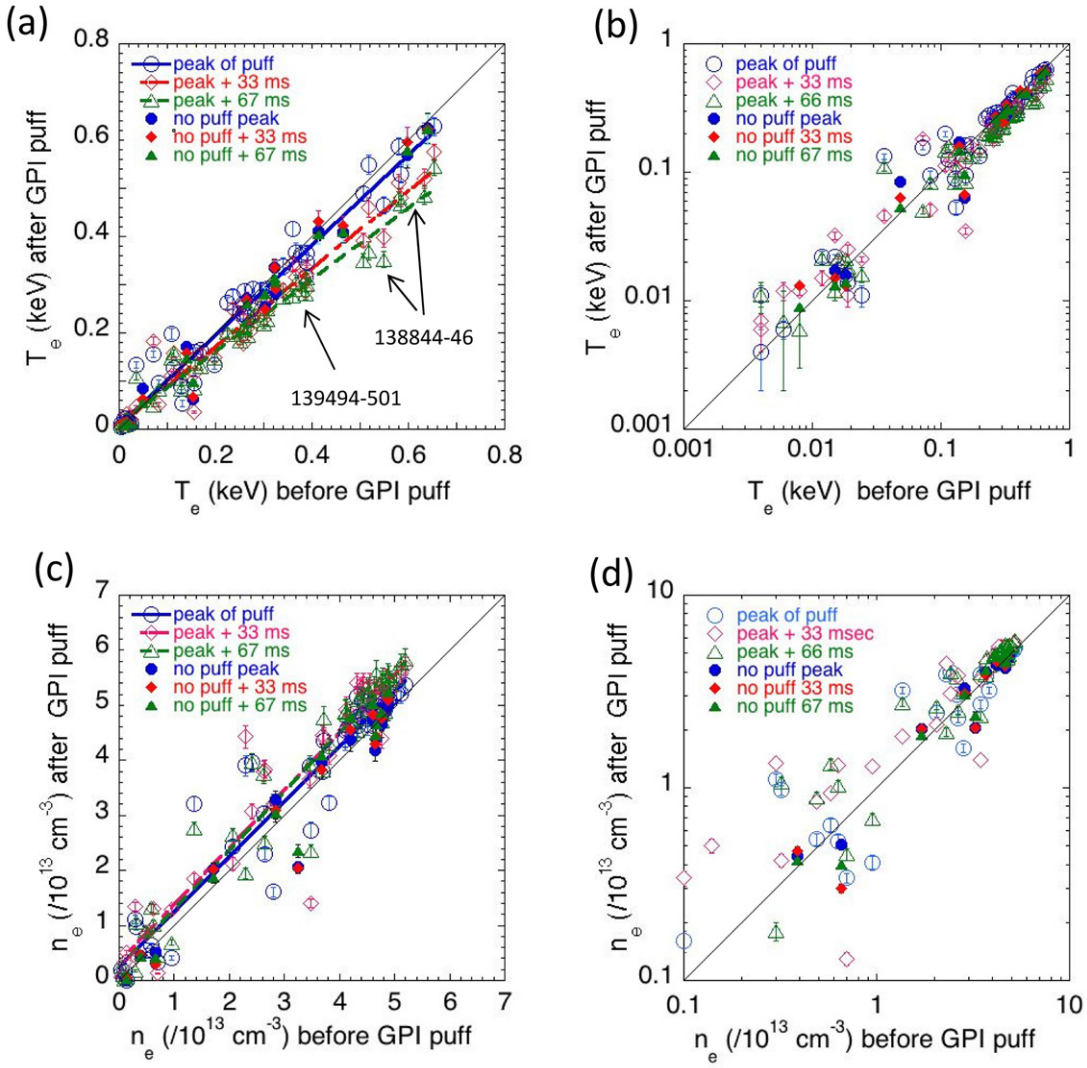

Figure 6. Comparison of T_e and n_e between the time just before (by ~10 msec) the GPI puff (horizontal axis) and three times after the GPI puff (vertical axis) for all points in the first two groups of shots in table 1. The same data is shown in a linear scale in (*a*) and (*c*) and a log scale in (*b*) and (*d*). Shots with no gas puff have solid symbols. There is a significant decrease in T_e at 33 and 66 ms after the peak of the puff for points at $T_e \geqslant 0.3$ keV, but not for $T_e \leqslant 0.3$ keV. There is a significant increase in the n_e in region where $n_e \geqslant 3 \times 10^{13}$ cm^{-3}at 33 and 66 ms after the peak of the puff, but little or no systematic change where $n_e \leqslant 3 \times 10^{13}$ cm^{-3} at these times. Data at 67 ms from groups 1 and 2 of table 1 are labeled with arrows in figure 6(*a*).

Table 3. Thomson data for linear fits and after/before ratios versus time during GPI puff.

	GPI peak (fit/ratio)	+33 ms (fit/ratio)	+67 ms (fit/ratio)
T_e (H-mode figure 6)	0.93/1.10	0.80/0.99	0.74/0.94
T_e (H-mode figure 7)	1.00/1.00	0.95/0.93	0.98/0.88
T_e (L-mode figure 7)	1.19/1.09	1.20/1.05	0.95/0.96
T_e (Ohmic figure 7)	0.92/0.81	0.90/0.66	0.81/0.61
n_e (H-mode figure 6)	1.00/1.23	1.04/1.34	1.07/1.29
n_e (H-mode figure 7)	1.07/1.06	1.11/1.13	1.33/1.06
n_e (L-mode figure 7)	1.08/1.15	1.25/1.16	0.88/1.30
n_e (Ohmic figure 7)	1.00/1.15	1.20/1.07	1.26/1.03

Figure 8(*a*) shows a typical image from the GPI diagnostic region of figure 1(*a*). The radial direction is nearly horizontal and the vertical direction is nearly poloidal (i.e. perpendicular to the local radial and toroidal directions), with the outward radial direction to the right, and the ion diamagnetic and ion grad-*B* drift directions downward. The Dα light emission is the vertical orange band just inside (i.e. left of) the magnetic separatrix shown by the dashed white line (calculated from EFIT). The projection of the RF antenna limiter is shown by the dotted line, and the GPI gas manifold is shown by the vertical solid line just outside the RF antenna.

The radial profile of GPI emission versus time was evaluated by averaging over the poloidal range $\pm$10 pixels around the vertical center of these images, i.e. between the two horizontal orange lines in figure 8(*a*). In figure 8(*b*) is the time dependence of the radial profile of the GPI light within this vertical band evaluated over the time of the puff, along with the separatrix location (black dashed line). This contour plot was averaged over ~1 ms in time to smooth out the turbulence. The peak of the GPI radial emission profile moves only about 1 cm radially during the duration of the puff, mainly following the small shift of the separatrix (note also that the poloidal profile does not vary significantly during the puff).

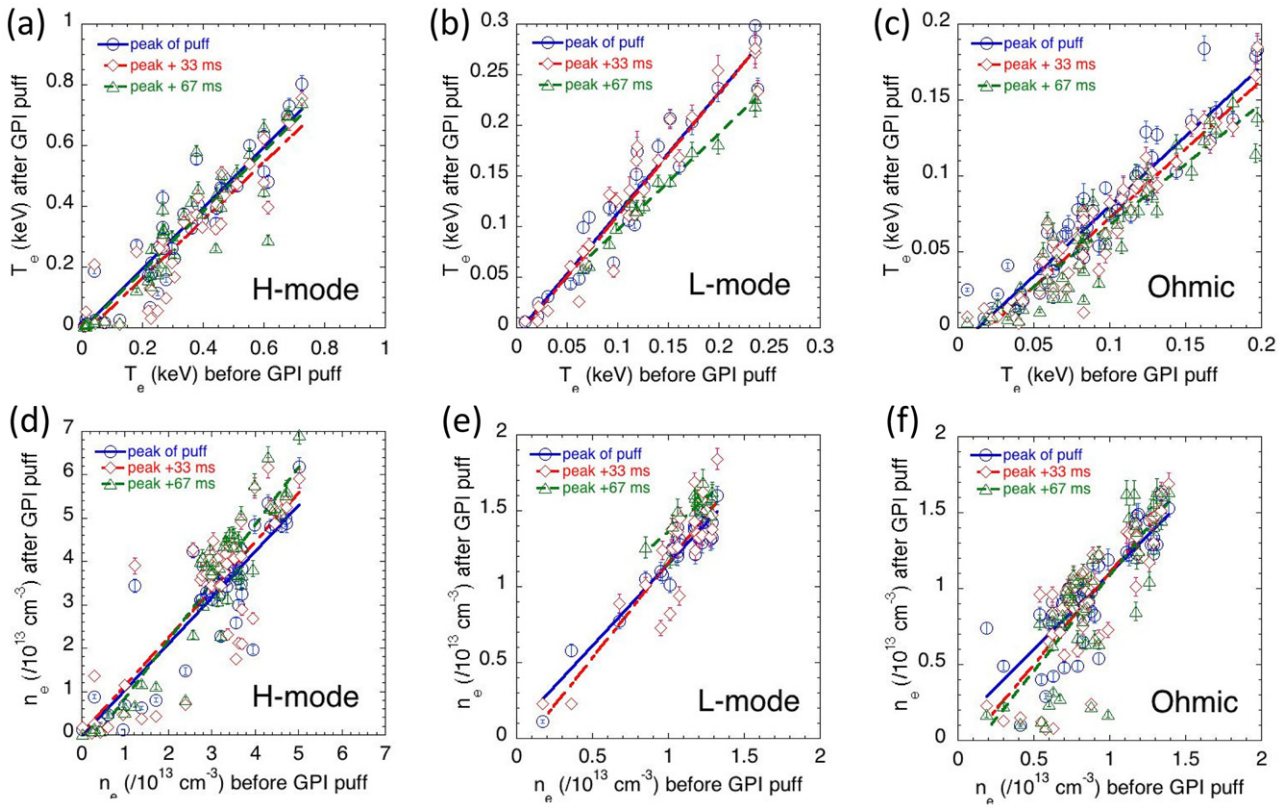

Figure 7. Additional Thomson scattering data in the same format as figure 6, but for the 3rd, 4th and 5th groups of shots of table 1 (which do not have comparison shots without a GPI gas puff). On the horizontal axes are the T_e and n_e just before (by $\sim$ 10 msec) the GPI puff, and on the vertical axes are the T_e and n_e at three times during the GPI puff. The T_e data is sorted in terms of H-mode shots in (*a*), L-mode shots in (*b*), and Ohmic shots (*c*), with the corresponding n_e data in (*d*)–(*f*). Linear fits are made to the data for each time and the slopes of these fits are shown in table 3. There is generally $\leqslant$25% systematic variation in the edge T_e and n_e due to the puff, although there is considerable random scatter in the data.

Figure 9 shows more about the time dependence of the radial profile of the GPI Dα light emission for the same shot as for figure 8. Figure 9(*a*) shows the time dependence of the GPI Dα light emission averaged over the whole GPI field of view, as in figure 2. Figure 9(*b*) shows the time variation of GPI radial profiles with respect to the time-averaged separatrix position, averaged over the vertical band of figure 8(*a*) and over 2.5 ms, with the relative time from earliest (black) to latest (red), following the color scale of figure 8(*b*). The radial peak of the GPI emission remains at 0.5 ± 0.5 cm inside the separatrix over this 80 ms period. Figure 9(*c*) shows the peak GPI location with respect to the time-averaged separatrix position (black), and the full-width at half-maximum (FWHM) of these GPI profiles (blue). The separatrix position versus time is shown by the red diamond symbols, and varies by $\leqslant$1 cm during the puff. The result of figure 9 is that the peak location and width of the GPI Dα profiles do not vary by more than $\sim$1 cm during the GPI puff in this case, even though the local Dα gas puff light varies by more than a factor of 10. A similar invariance of the GPI profile during the puff was noted previously in a different set of NSTX discharges [4]. Note that the GPI profile width does decrease from before the puff to after the start of the puff at 0.593 s, since without the puff the Dα emission is not toroidally localized.

Figure 10 shows the GPI signal levels, peak locations and widths versus time for a set of six H-mode shots, two from each of the first three shot groups of table 1. These GPI analyses were also averaged over the central vertical region defined by the horizontal lines in figure 8(*a*), and the peak locations in figure 10(*b*) and widths in figure 10(*c*) are plotted only after the GPI signal is significantly above the Dα background light. There is no systematic variation in the GPI peak location or width over the time during which the GPI signal level rises by at least a factor of $\sim \times$ 5–6 before its peak, or during the time over which the GPI signal level fall by a factor of $\sim$3 after the peak. Thus there is no clear evidence for a systematic variation in the local plasma parameters due to the puff itself; for example, due to a local increase in density, which would tend to shift the emission peak radially outward (see section 3.1). For the Ohmic and L-mode shots of table 1 there is sometimes up to a $\sim$2 cm shift of the peak GPI location versus time during the puff, but this is mainly correlated with shifts in the separatrix position during these relatively non-stationary discharges, and not systematically correlated with the puff itself.

2.4. GPI turbulence analysis

Figure 11(*a*) shows an example of the time dependence of the GPI signal within the small 1.5 cm square region shown in figure 8(*a*), which is centered at a radius 1 cm inside the separatrix position for this shot. This signal smoothed over 1 ms is shown by the orange line. The time dependence of this Dα signal is similar to the average over the whole frame

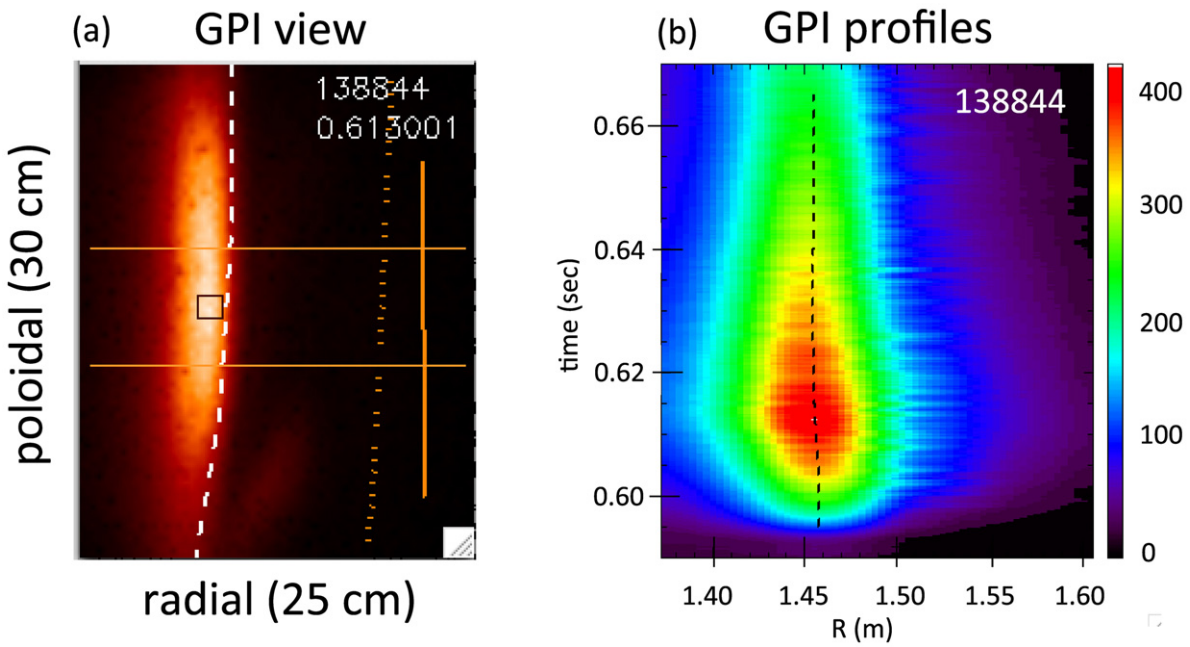

Figure 8. (*a*) shows a typical image of the ~25 cm × 30 cm region of the GPI gas puff just above the outer midplane of NSTX, with the radial direction is approximately horizontal (outward to the right), and the vertical direction approximately poloidal (downward in the ion grad-*B* drift direction). The Dα light emission is the vertical orange band just inside the separatrix, which is shown by the dashed white line. The projection of the RF antenna is shown by the dotted orange line, and the GPI gas manifold is shown by the vertical solid line. The vertical region used to evaluate the radial profile of GPI emission is between the two horizontal red lines, and the small black 1.5 cm × 1.5 cm square 1 cm inside the separatrix is used to evaluate the turbulence. In (*b*) is the GPI signal level versus time and local major radius for this shot, along with the separatrix, shown as a black dashed line. The false-color relative Dα brightness level scale is at the right.

for a similar shot in figure 9(*a*), and to the average over the vertical middle of the image in figure 10(*a*). Figure 11(*b*) shows the frequency spectrum of the normalized amplitude fluctuations in the GPI signal in this square region versus time, i.e. of the signal divided by its value smoothed over 1 ms, with the spectral amplitude scale shown by the color bar at the upper right. In this example the normalized fluctuation spectrum is very similar from the very beginning of the puff (0.595 s) through 55 ms after the peak of the puff (0.670 s). For other radii and other shots the spectra are not always so constant versus time, but there is no general systematic variation of the spectrum shape versus time during these gas puffs.

Figure 12 shows the analysis of several turbulence quantities for the same six H-mode shots used for figure 10, averaged over the same 1.5 cm square regions located 1 cm inside the separatrix such as shown by the black square in figure 8(*a*). Figure 12(*a*) shows the GPI Dα light versus time. Figures 12(*b*) and (*c*) show the relative GPI fluctuation levels (rms/mean) and autocorrelation times (FWHM), neither of which show any systematic variation during these gas puffs. Figures 12(*d*) and (*e*) show the correlation lengths as evaluated between similar square regions centered 1.5 cm apart around the regions used for figures 12(*a*)–(*c*), assuming Gaussian correlation function as in [42]. There is also no systematic variation in these correlation lengths over the time of these puffs. Finally, figure 12(*f*) shows the poloidal velocity $V_{\rm pol}$ calculated as in [42] using data from individual pixels and time delays of up to 10 μs. Again, there was no systematic variation in these turbulence velocities over the time of these puffs. The radial velocities (not shown) were much smaller than the poloidal velocities for these H-mode cases (within ± 1 km s^{-1} of zero), and also showed no variation with the GPI puff.

The conclusion from this analysis is that the local edge turbulence as measured by the GPI diagnostic itself does not vary as the influx rate of the gas puff varies by at least a factor of ×5, at least for H-mode discharges. This implies that the GPI gas puff itself does not significantly perturb the edge turbulence in these typical cases. It is interesting to note that the edge turbulence is not substantially different among the six shots shown in figure 12, which have a range of NBI power from 2–6 MW along with different global parameters (see table 1). This shows that the edge turbulence in NSTX is relatively insensitive to the edge plasma parameters, at least for these H-mode plasmas.

2.5. Other diagnostic data

Figure 13 shows several other signals as a function of time during the GPI puff for the same shots as in figure 2(*a*), in which one shot has no gas puff (#138843) and the three successive shots have a GPI gas puff (top panel). Recall that these are the shots which showed the largest effect of the gas puff on the edge plasma temperature among the first two groups of shots, as shown in figure 6(*a*). Figure 13(*a*) shows the GPI gas puffs, and figure 13(*b*) shows an ultra-soft x-ray signal chord with a tangency radius 3.5 cm inside the separatrix [43], which has only a slight increase at the time of the puff. Figure 13(*c*) shows the outer separatrix locations, which have no significant variation during the puff. Figure 13(*d*) shows Dα signals from the lower divertor region, which do have a significant increase with the GPI puff, most

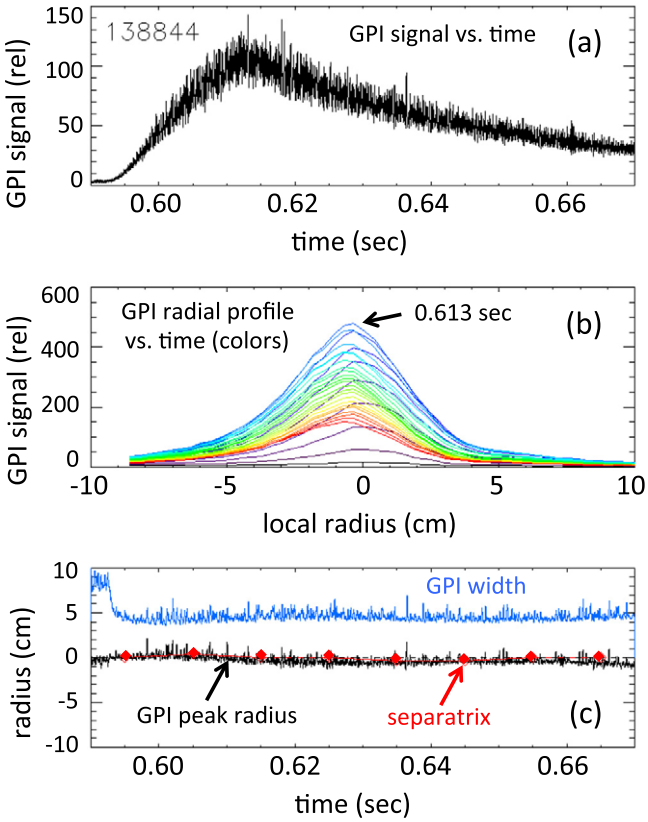

Figure 9. Time evolution of the Dα light emission for one of the shots in the first group in table 1. (*a*) shows the time dependence of the GPI Dα light emission averaged over the whole GPI field of view. (*b*) shows the variation of GPI radial profiles over this time, spatially averaged over the central vertical region defined by the horizontal lines in figure 8(*a*) and plotted every 2.5 ms, with the relative time from earliest (black) to latest (red), following the color scale of figure 8(*b*). (*c*) shows the peak location (black) and FWHM (blue) of these GPI profiles with respect to the average local separatrix position at the GPI view (zero on this scale), and the EFIT separatrix position versus time (red line with diamonds).

likely due to parallel transport of ions from the GPI puff region to the divertor plate. Figure 13(*e*) shows the total radiated power in the main plasma volume, which has little or no change with the puff. Finally, in figure 13(*f*) are the neutron signals, which decrease by ~10–20% by ~50 ms after the peak of the puff, perhaps reflecting the decrease in electron temperature shown in figure 4. In general, these other diagnostic signals (except for the divertor Dα) show only a small effect of the GPI puff on both the edge and core plasma.

Figure 14 shows the edge ion temperature and rotation speed measured for all of the shots in table 1 using the NSTX edge rotation diagnostic, which is based on passive visible spectroscopy of C III [44]. The ion temperature in figure 14(*a*) and toroidal velocities in figure 14(*b*) were evaluated at the peak of the radial emission profile of this line, which is typically located a few centimeters inside the separatrix. Linear fits to these data are shown by the lines, which show little or no systematic change in T_i or V_{tor} during the GPI puff. A similar plot of V_{pol} shows no significant variation with the puff, but with V_{pol} within $\pm 20\,\mathrm{km\,s^{-1}}$ of zero. Note that the poloidal position of the measurements in figure 14 was near the outer midplane, but its toroidal position was ~90° away from the GPI puff. Thus these T_i and V_{tor} data are taken far from the magnetic flux tubes going through the GPI puff, and so do not exclude a possible local modification on the GPI gas puff flux surfaces. The active CHERS data was not available due to interference of the GPI puff with the background CHERS signal.

Figure 15 shows data from the beam emission spectroscopy (BES) diagnostic, which measures the Dα light emission from the NBI. Figure 15(*a*) shows an increase in the BES signal level in one channel versus time, which follows the Dα emission from the GPI puff in shown in figure 15(*d*), to within the uncertainty in the mutual timing. This particular BES signal is from ~3 cm inside the separatrix from a sightline located ~40 cm from the GPI gas puff, as shown in figure 1. This BES signal and its fluctuation level in figure 15(*b*) are apparently affected by the neutral deuterium density due to the GPI puff in its vicinity, most likely due to the collision of beam ions with cold edge neutrals. The relative fluctuation levels (RMS/mean in %) in this BES channel above either 0.2 or 4 kHz are shown in figure 15(*c*). The relative fluctuation level integrated over $\geqslant$4 kHz is not significantly affected by the GPI puff, but when the high-pass filter is at $\geqslant$0.2 kHz there is an increased fluctuation level in BES during the GPI puff in these shots (although not in other shots). A detailed comparison of BES and GPI fluctuations will be presented elsewhere [45]. Signals from the high-k scattering diagnostic viewing nearest the edge at $R \sim 138 \pm 2$ cm also show no qualitative change with the GPI puff, e.g. at $k_\perp \rho_s = 16$. There is also no visible effect of the GPI gas puff on the MHD activity as measured by the magnetic fluctuation coils inside the vacuum vessel.

2.6. L–H transition and ELMs

None of the 27 shots in table 1 had an L–H transition or an H–L transition during the time of the GPI gas puff, which shows that this puff does not necessarily trigger either a transition or a back-transition in NSTX. There were 23 other shots in the 2010 run which did have an L–H transition during the GPI puff duration period, mainly because the GPI puff was purposely triggered to catch these transitions. In those cases the time of the L–H transitions varied between ~18–105 ms after start of the puff, i.e. without any clear correlation to the influx rate from the GPI puff. Earlier studies of the L–H transition in NSTX also showed no effect of the GPI puffing on the L–H transition [46].

Similarly, there is no evidence that the GPI gas puff affects ELMs in NSTX. The shots in table 1 were chosen to avoid ELMs during the GPI puff, therefore the puff does not necessarily trigger ELMs. However, there were many other shots with ELMs during the GPI puff (e.g. in [4]), and previous studies were made of the 2D structure and motion of ELMs using GPI data [47, 48], so the puff does not suppress ELMs either. It is not clear why injection of small deuterium pellets can trigger ELMs [37], while a gas puff with a similar time-averaged neutral influx does not.

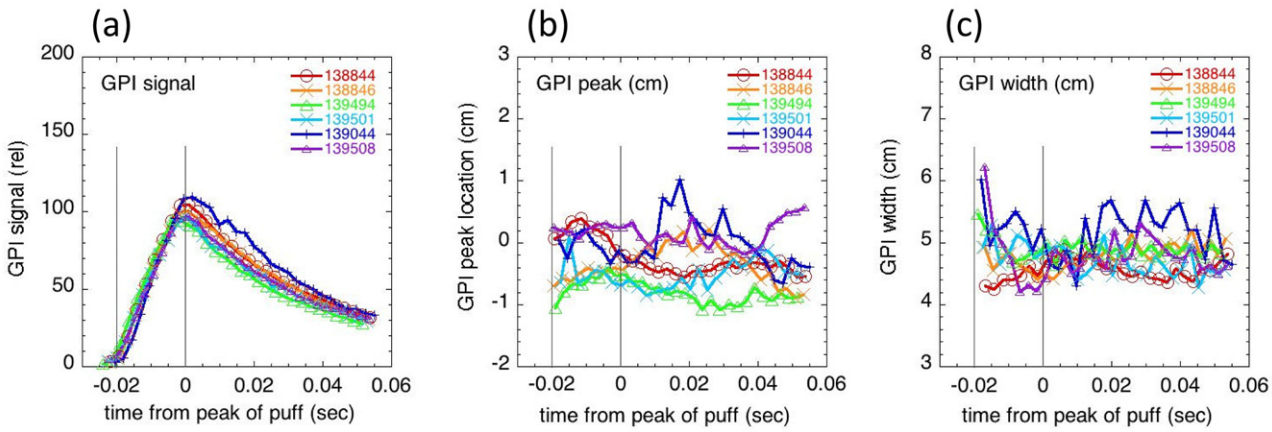

Figure 10. For six of the H-mode shots of table 1, (*a*) shows the GPI signal levels versus time, and (*b*) and (*c*) show the radial peak locations and widths (FWHM) of the Dα light emission versus time. All these are averaged over the central vertical region defined by the horizontal lines in figure 8(*a*), and plotted with respect to the peak time of the GPI emission signals. The vertical lines show beginning of the puff and its peak 20 ms later. There is no systematic time variation of the GPI peak location or width versus time during the puff in these cases.

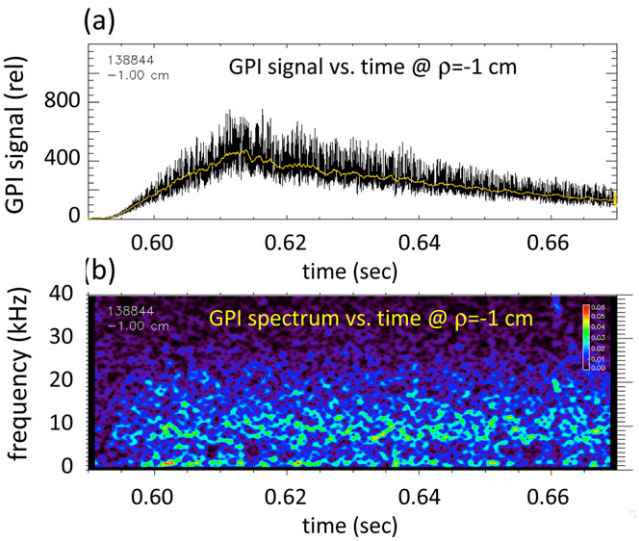

Figure 11. (*a*) shows the time dependence of the GPI signal within the small 1.5 cm square region shown in figure 8(*a*), which is centered 1 cm inside the average separatrix position for this shot. Overlaid in orange is this same signal smoothed over 1 ms. (*b*) shows the frequency spectrum of the amplitude fluctuations in the normalized GPI signal in this region versus time. The amplitude scale is shown by the color bar at the upper right. There is no significant variation in the turbulence spectrum over time for this shot.

3. Modeling

At present there is no complete model for the effects of a deuterium gas puff on these NSTX plasmas. Sections 3.1 and 3.2 apply the existing codes DEGAS 2 and UDEGE to partially model one shot in this run. Section 3.3 then describes simplified generic estimates for the local and edge effects of this gas puff, including a discussion of their limitations.

3.1. DEGAS 2 modeling

3D DEGAS 2 simulations for four times during the H-mode shot 138846 have been run in the manner described in [4]. These simulations use an EFIT equilibrium to define the flux surface shapes in the vicinity of the GPI viewing area. The electron density and temperature values obtained from the Thomson scattering diagnostic are mapped onto these, assuming that they are constant on flux surfaces. One improvement relative to the procedure in [4] is that data from the CHERS diagnostic are used to estimate a fixed ratio of the deuterium ion to electron density ratio. Since we have no *a priori* reason to believe that T_i differs significantly from T_e and since the CHERS data do not extend into the GPI emission region, we assume $T_i = T_e$. Note that this DEGAS 2 modeling does not determine the response of the plasma to the GPI gas puff.

Deuterium molecules are sampled randomly from a 300 K thermal energy and cosine angular distribution across ten 2×2 cm squares that represent the GPI gas manifold; the squares are aligned with the pitch of the actual manifold. As the molecules penetrate the plasma, they undergo ionization, dissociation and elastic scattering; resulting molecular ions are assumed to be ionized, dissociated or recombined immediately. Any product atoms are then tracked through the plasma and interact with it via ionization and CX. The DEGAS 2 simulation volume covers the entire region $R = 1.2 - 1.7$ m in major radius, $z = -0.4$–0.4 m in the vertical direction (see figure 1(*a*)), and a toroidal angular range of 90° around the gas manifold. The principal output of the DEGAS 2 calculations is the simulated view of the GPI camera obtained by integrating the Dα emission from atoms and molecules along chords corresponding to each of the camera's 80 × 64 pixels. The reader is referred to [4] for additional details.

To estimate the dimensions and volume of the Dα emission region, we construct 2D slices through the simulation volume both parallel and perpendicular to the gas manifold, i.e. in the local poloidal or bi-normal direction for the parallel slice, and in the local magnetic field direction for the perpendicular slice. From each, we obtain the FWHM of the emission profile. The widths parallel to the manifold and the magnetic field are comparable, $L_o \sim 15$ cm. The radial width is much more narrow, 2–3 cm, reflecting the steepness of the H-mode plasma profiles. This radial width is somewhat less than the measured width of ~4–5 cm for this shot in figure 10(*c*), probably due

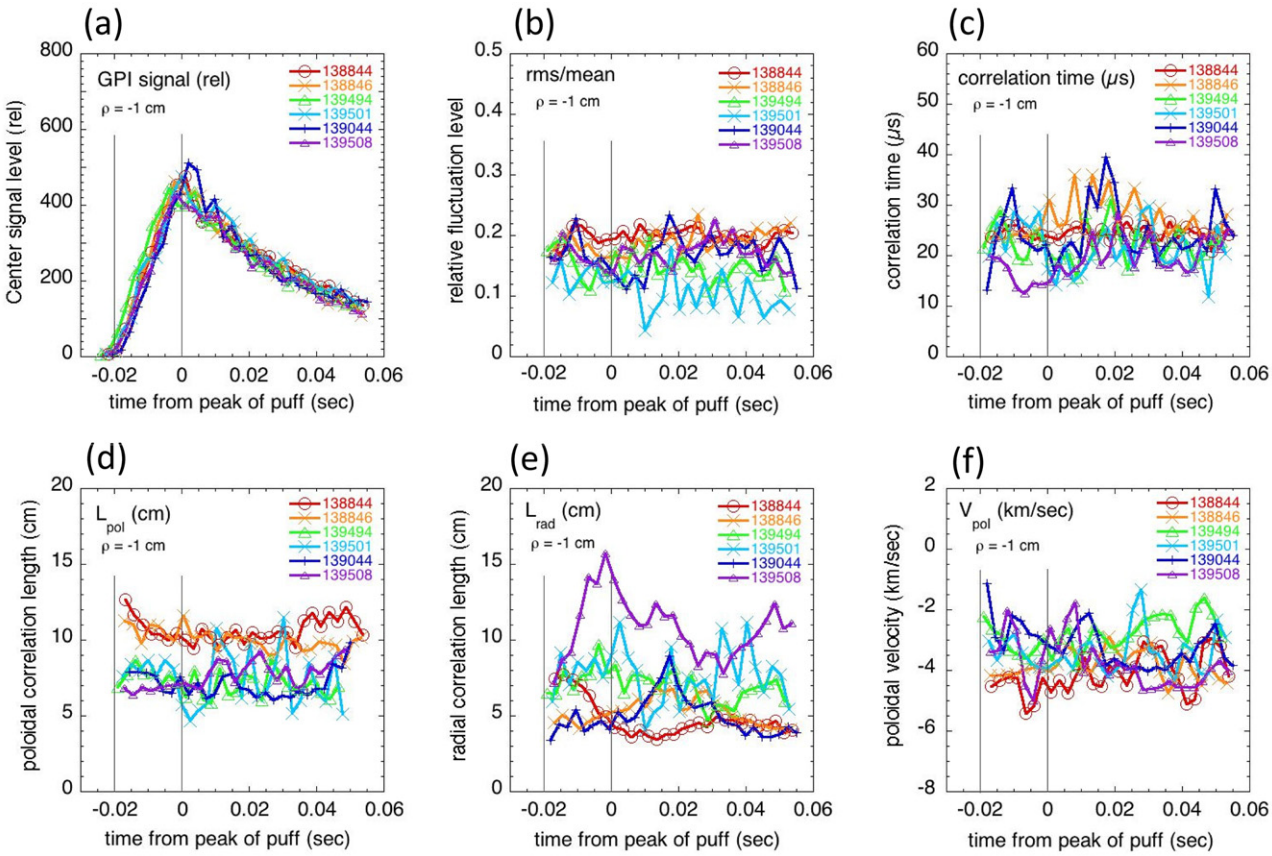

Figure 12. Several turbulence quantities as a function of time for the same six H-mode shots used for figure 10, averaged over 1.5 cm square regions located 1 cm inside the separatrix. The time is measured with respect to the peak of the GPI signal levels. (*a*) shows the GPI signal levels, (*b*) shows the rms/mean, (*c*) shows the autocorrelation times, (*d*) and (*e*) show the poloidal and radial correlation lengths, and (*f*) shows the poloidal velocities. There are no significant variations in the edge turbulence versus the time over the duration of these GPI puffs.

to the broadening effects of the finite toroidal width of the gas cloud and plasma turbulence in the actual shot. The overall shape of the Dα emission region is that of a disk, i.e. a flat cylinder ~15 cm along the magnetic field by ~15 cm poloidally by ~2–3 cm radially. The corresponding estimate of its volume of the Dα emission region is 300–500 cm^3, and the maximum neutral density within this cloud is $\sim 5 \times 10^{12}$ cm^{-3} at the time of the peak in the GPI puff.

The volumetric sources of plasma particles and energy computed in these simulations can be averaged over flux surfaces within the simulation volume for the purpose of estimating the global impact of the gas puff on the plasma. Figure 16(*a*) shows radial profiles of these energy source rates for the simulation of 138846 at the time of the peak puff rate, 0.615 s, and scaled to a peak neutral gas source rate of 6.6×10^{21} atoms s^{-1}; the volumetric photon emission rate is included in the figure for reference. These source rates can in turn be summed over the volumes inside and outside the separatrix, as well as over the entire volume, as shown in table 4. The calculated ionization rate inside the separatrix is 1.8×10^{21} atoms s^{-1}, which is 27% of the neutral gas puff rate. This is somewhat higher than estimates of 'fueling efficiency' of 0.05–0.20 deduced for other gas puffing systems in NSTX [49].

Note that these DEGAS 2 runs have been designed to simulate the plasma–neutral interactions only in the vicinity of the GPI camera view and that a significant fraction (~1/3) of the neutral atoms and molecules leave the simulation volume without being ionized. Note also that the dividing line between source rates inside and outside the separatrix in figure 16 and table 4 depends on the accuracy of the EFIT equilibrium reconstruction of the separatrix location, which is uncertain by up to about ±2 cm.

The electron energy losses are roughly evenly split between those due to atoms (ionization, line radiation) and molecules (dissociation and ionization), and total ~6.5 kW inside the separatrix and 14.5 kW outside the separatrix, for a total electron energy loss of 21 kW. Overall, the ions lose 18 kW, effectively heating deuterium atoms via CX, but gain 13 kW of this back when those atoms are ionized, because the warm atoms then become ions (again). Therefore the direct energy loss rate due to atomic physics processes in the gas cloud is negligible compared with the power flow from the main plasma through the edge flux surfaces, which is ~4 MW for this shot.

DEGAS 2 simulations of shot 138846 were done at four times relative to the peak time of the puff (0.615 s): −20, 0, +30 and +70 ms, based on the Thomson scattering measurements of n_e and T_e made at the other side of NSTX. Radial profiles from both the simulated and experimental camera images are obtained by integrating over 20 pixels around the vertical center of the frame, i.e. between the red lines in figure 8(*a*). The radial

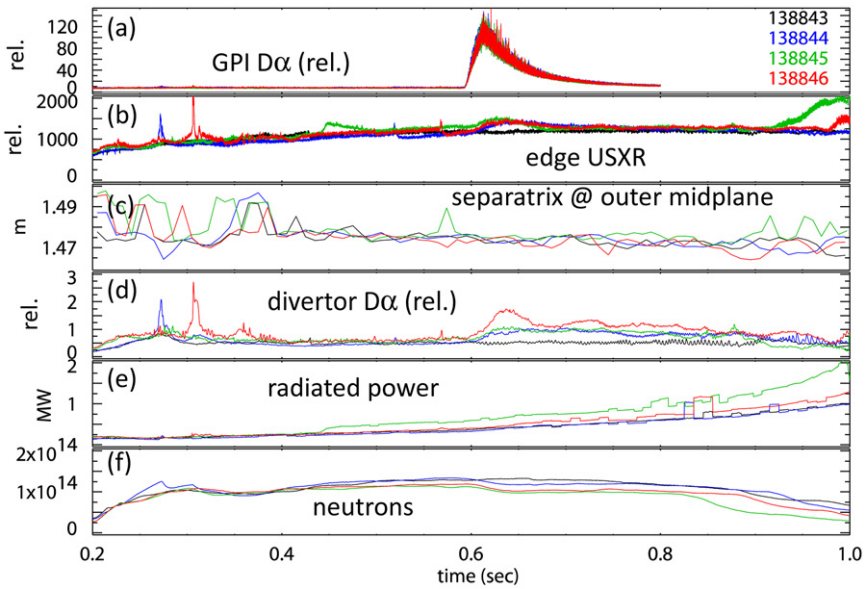

Figure 13. Several other diagnostic signals as a function of time across the GPI puff for the same shots as in figure 2(*a*), where one shot has no puff (#138843) and the three successive shots have a similar puff. (*a*) shows the GPI Dα signals, (*b*) shows the edge USXR signals, (*c*) shows the separatrix positions, (*d*) shows the divertor Dα signals, (*e*) shows the total radiated power, and (*f*) shows the neutron rates. In general, these signals are consistent with a relatively small effect of the GPI puff on both the edge and core plasma, except for the divertor Dα signals.

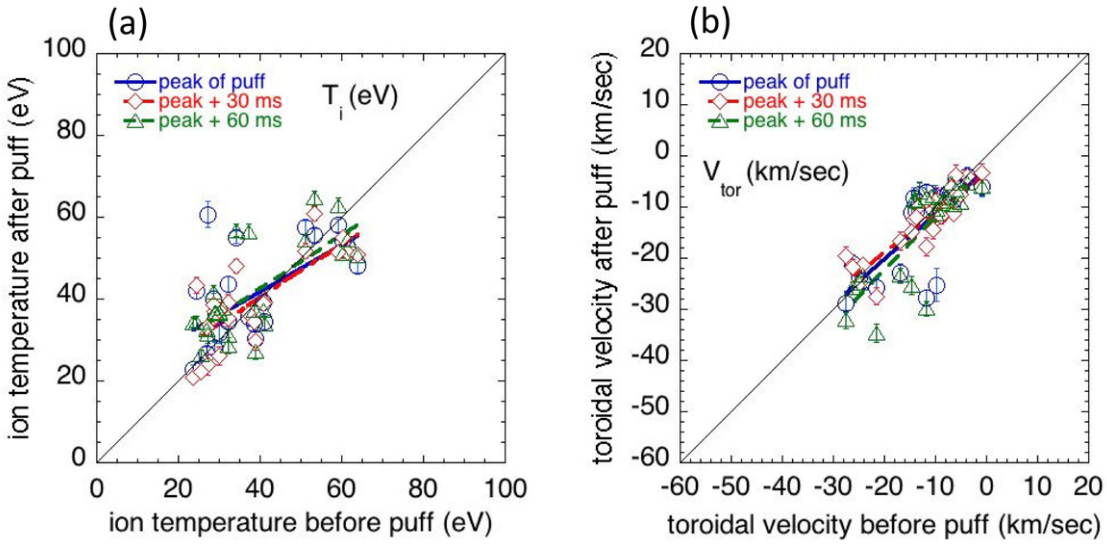

Figure 14. Edge ion temperature (*a*) and toroidal rotation speed (*b*) measured for all shots in table 1 using passive visible spectroscopy of the C III line, which is located just inside the separatrix (but not on the same B field line as the GPI puff). This analysis is plotted the same way as in figures 6 and 7, with the values just before (by $\sim$ 10 msec) the start of the puff on the horizontal axis and the values at three times after the start of the puff on the vertical axis. There is little or no systematic change in T_i or V_{tor} after the puff, although there is considerable shot-to-shot scatter. The lines show linear fits to the data.

locations of the Dα peaks of these profiles, mapped to midplane and relative to the separatrix, are shown in figure 16(*b*). The error bars reflect an uncertainty of ± 1 pixel (0.3 cm), based on [4, 50]. Note however that the radial separation between Thomson edge channels is 2 cm, so any resolution finer than this is based on interpolation.

The simulated DEGAS 2 radial profile peak locations for three of the four radial points are within the error bars of the observed GPI peak locations, as was also found previously for four other H-mode shots [4]. The largest deviation in the DEGAS 2 peak location in figure 16(*b*) is at +30 ms (0.645 s), where it was $\sim$2 cm farther radially outward than the observed GPI peak in this shot. The location of the Dα peak in the DEGAS 2 simulation depends on the T_e profile through the atomic physics of D atoms (which is well known), but is also uncertain due to possible time-dependent fluctuations in T_e, to the limited spatial resolution of the Thomson measurements, and possibly to a difference between the n_e and T_e in the GPI gas cloud and the Thomson scattering measurements on the same flux surfaces. Note that the radial excursion of the simulated peak location in shot #138846 tracks the separatrix temperature (dashed line in figure 16(*b*)), allowing us to use

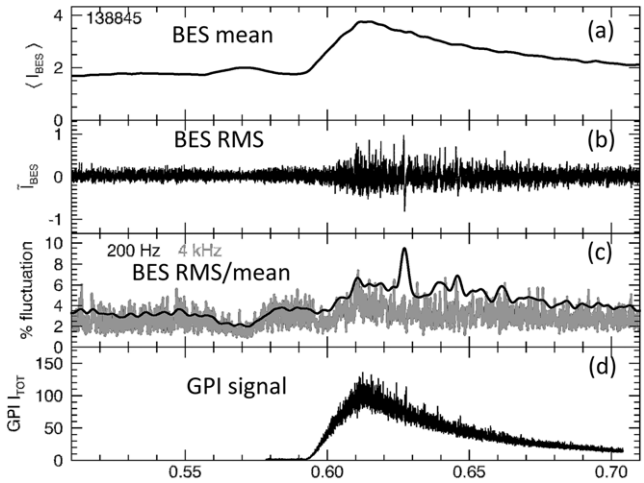

Figure 15. Data from the BES diagnostic, which measures the Dα light emission from the NBI, showing in (*a*) and (*b*) an increase in BES signal level and RMS fluctuation level at ~3 cm inside the separatrix, which correlate with the GPI puff signal (*d*). This BES sightline is near the GPI gas puff (see figure 1), and its signal level is affected by the increase in neutral density due to the GPI puff. The relative fluctuation levels (RMS/mean in %) in BES above 0.2 and 4 kHz are shown in (*c*). The relative fluctuation level at low frequencies (~0.2–4 kHz) is slightly affected by the GPI puff in these shots.

the Thomson scattering profiles of similar shots to estimate the Dα peak location for those shots without doing additional DEGAS 2 simulations. Since the Thomson scattering profiles for the similar shots 138844 and 138845 do *not* have same time dependence as 138846 for the separatrix temperature over the GPI gas puff time of 0.590–0.680 s (see figure 5), we conclude that the 2 cm discrepancy seen at 0.645 s is most likely due to a random turbulent fluctuation seen by the Thomson scattering for this point in space and time, which is not accounted for in the depicted error bars [50].

A rough evaluation can be made of the expected radial shift of the emission peak in response to a local change in the density. The variation of the Dα emission rate with n_e and T_e for plasma parameters typical of the emission peak (e.g. $T_e \sim$ 30–70 eV) is expected to be $n_e^{0.4}$ if the temperature change is inversely proportional to the density change. Using this scaling and the plasma gradients near the peak, we find that a doubling of the density would shift the emission peak by ~0.5 cm. This is marginally within the resolution of these measurements, so that the Dα profile measurement can only discern a local density change larger than a factor of 2. Estimates of the gas puff effects on the local plasma parameters are further discussed in section 3.3.

3.2. UEDGE modeling

UEDGE, a 2D (axisymmetric) multi-fluid edge transport code [51], was used to evaluate the effects of the GPI gas puff on the NSTX edge plasma for shot 138846 (same shot as for section 3.1). A narrow slice of the edge and SOL is captured; at the outer midplane, the grid extends from 1.92 cm inside the separatrix to 0.65 cm into the SOL. The separatrix location is calculated self-consistently with the expected SOL heat flux and is ~1 cm farther in than the EFIT separatrix used

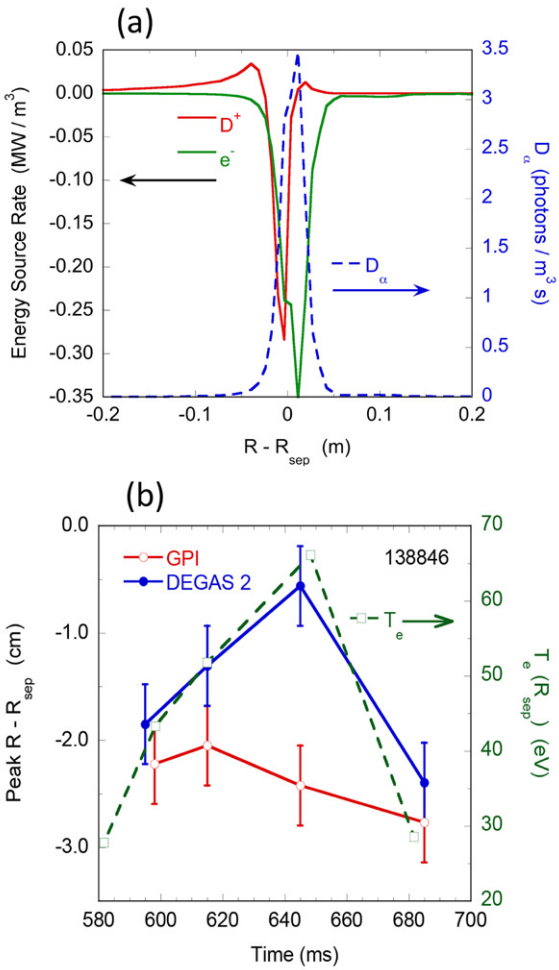

Figure 16. In (*a*) are volumetric energy source rates from DEGAS 2 simulation of shot #138846 at the peak of the gas puff (0.615 s), averaged over flux surfaces within the simulation volume and mapped to major radius at midplane. The corresponding Dα emission rate is included for reference. In (*b*) are the radial locations of simulated (blue) and experimental (red) emission peaks relative to the separatrix. The electron temperature at the separatrix is included for reference. The radial difference of ~2 cm between DEGAS 2 and GPI at 645 ms is relatively small (comparable to the Thomson spatial resolution), and most likely due to a random fluctuation in edge profiles.

in DEGAS 2. Parallel transport is treated with the flux-limited Braginskii equations [52], perpendicular transport is modeled with assumed anomalous perpendicular diffusivities (with no pinch) to fit the pre-puff plasma profiles, and a fluid neutral model employed. Carbon radiation is included, assuming a fixed 5% carbon concentration, consistent with midplane C^{6+} density measurements. Radially varying diffusivities are adjusted such that UEDGE midplane temperature and density profiles approximately match midplane Thomson data. This simulation also includes the particle source from the center stack gas puff and NBI, which were the same for shots with and without the GPI gas puff, and an assumed divertor recycling coefficient of 0.9.

After establishing a steady-state solution, an axisymmetric model of the GPI gas puff is introduced (see below), and the time-dependent edge plasma behavior is tracked. This gas

Table 4. DEGAS 2 138846 @ 0.615 s volume integrated source and loss rates.

	Peak ion source rate ($D^+ s^{-1}$)	Peak ion power loss (kW)	Peak electron power loss (kW)
Inside separatrix	1.8×10^{21}	4.0	6.5
Outside separatrix	2.6×10^{21}	0.05	14.5
Total	4.4×10^{21}	4.0	21

puff rate rises linearly for 20 ms to $2.6 \times 10^{21}\ s^{-1}$, which is the peak deuterium gas flux into the UEDGE domain based on DEGAS 2 results (section 3.1). After the peak, the puff decays exponentially with a 50 ms decay time.

The GPI gas puff is modeled in UEDGE by an axisymmetric neutral deuterium influx at the low-field-side over a poloidal length of ~45 cm. The poloidal distribution of the ion density near the separatrix in UEDGE is calculated self-consistently using the neutral sources, radial transport, and recycling at the divertor, and has about a factor-of-two variation with poloidal angle. The shape of the poloidal distribution of the ion density near the separatrix is roughly constant during the GPI gas puff, since the edge poloidal ion transit time is much smaller than the gas influx timescale, e.g. the ion transit time over a typically parallel connection length of $L \sim 5$ m at an ion energy of ~50 eV is ~0.1 ms.

The UEDGE modeling shows a relatively strong edge plasma response, as seen for example by the ion and neutral densities and ion and electron temperatures evaluated near the outer midplane separatrix in figure 17. There is a similar relative density rise at other radial and poloidal locations within the UEDGE modeling region. The calculated ion density in figure 17 increases by ~50% by the time of the peak of the puff, and by 30 ms after the peak of the puff the calculated ion density at the separatrix rises by about a factor-of-two from 0.8×10^{13} to $1.5 \times 10^{13}\ cm^{-3}$, i.e. $\delta n = 0.7 \times 10^{13}\ cm^{-3}$. The neutral density due to the gas puff at the separatrix rises to $\sim 5 \times 10^{10}\ cm^{-3}$, but the local neutral influx due to the gas puff is $\leqslant$25% of the calculated neutral influx due to recycling at the divertor.

This calculated rise in edge density can be interpreted in terms of an edge particle confinement time $\tau_{p,UEDGE} = (\delta n V_{UEDGE})/\Gamma_{o,in}$, where $V_{UEDGE} = 2.5 \times 10^6\ cm^{-3}$ is the simulation volume and $\Gamma_{o,in} = 1.3 \times 10^{21}\ s^{-1}$ is an average rate of GPI puff ionization inside the separatrix for the modeled time period. This results in a $\tau_{p,UEDGE} \sim 10$ ms, which is significantly higher than the estimated edge energy confinement time (see section 3.3). This relatively large edge density rise is partially due to the large recycling at the divertor plate and to the divertor detachment, which occurs in this simulation due to the GPI puff, but which is not seen experimentally in these discharges.

These factor-of-two changes in edge density and temperature in UEDGE with gas puffing are apparently somewhat larger than the measured $\leqslant$20% changes seen in the edge Thomson scattering data of figures 4–7 and table 3. However, given the limitations of the UEDGE model and the limited available experimental data, it is not possible at this time to make a quantitative comparison between the two. Clearly it would be preferable to model the gas puff as a localized source in 3D, but this is not yet possible in UEDGE. Thus this simulation should be considered as a first attempt at modeling this gas puff, and additional physical effects missing from this preliminary simulation might be unveiled by future model refinement.

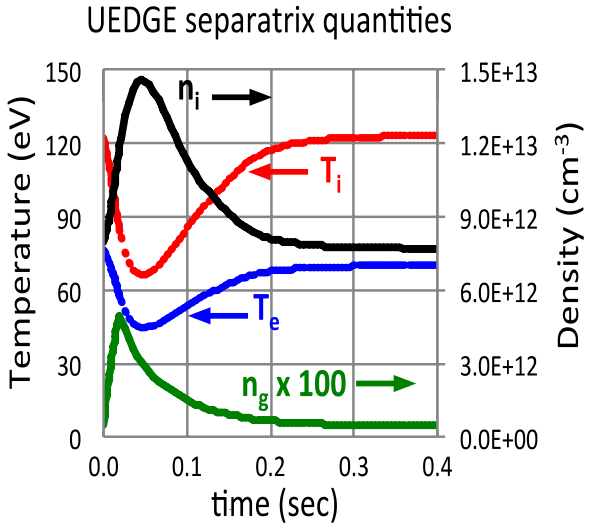

Figure 17. Results from UEDGE modeling of shot #138846, showing the calculated response at the separatrix for a simulated GPI gas puff. The neutral gas density (n_g) closely follows the rise and fall of the gas puff rate, and the deuterium ion density (n_i) rises for 30 ms after the peak puff due to the recycling and divertor detachment in the simulation. As a consequence the ion and electron temperature decrease by a similar fraction, since the total energy in the edge plasma is nearly constant in this simulation.

3.3. Simple estimates for the edge effects of the gas puff

This section describes simple estimates for the expected local and flux-surface averaged effects of the gas puff on the density and temperature in a typical discharge in this experiment. We first estimate the maximum *local* (i.e. *in 3D)* density perturbation expected within the gas cloud itself for shot #138846, which was modeled in sections 3.1 and 3.2. Newly created ions are assumed here to be lost from the neutral gas cloud only by parallel motion along B with a typical deuterium ion sound speed of $c_s \sim 5 \times 10^6\ cm\ s^{-1}$ assuming $T_e \sim 50$ eV near the peak of the ionization rate (i.e. $c_s/2$ in both directions). If there is no return of these ions to this birth region, the local density rise within the ionization volume V_o for a neutral influx rate of Γ_o should be $\delta n_{local} \sim (\Gamma_o/V_o)(L_o/c_s)$, where L_o is its cloud length along B, with typically $L_o \sim 15$ cm and $V_o \sim 300$–$500\ cm^3$ from DEGAS 2 modeling (section 3.1). The ion loss time from this volume is $(L_o/c_s) \sim 3\ \mu s$, i.e. less than the turbulence timescale, so the turbulent motion should not affect this loss rate; also, toroidal ion motion at ~10 km s^{-1} should only move ions ~3 cm within this time. Given a peak ionization rate of $\Gamma_o \sim 4.4 \times 10^{21}$ atoms s^{-1} over the whole gas cloud (table 4), the density rise within the GPI gas cloud at this peak time should then be $\delta n_{local} \sim 3 \times 10^{13}\ cm^{-3}$, and the radial profile of this rise should be the similar to the photon emission profile shown in figure 16(*a*). This is somewhat smaller than

the edge pedestal density at the peak time of the puff in this shot, but larger than the density at the separatrix, as shown in figure 5(*b*). Unfortunately there is no direct measurement of the local rise in density within the gas puff region with which to compare this estimate.

On a longer timescale, the ions born inside the separatrix will travel along B and fill up the volume of the flux surfaces on which they were born, which extends roughly $\delta r_{\rm in} = 3$ cm radially inside the separatrix at the outer midplane (figure 5(*b*)) over a volume of $V_{\rm edge} \sim (4\pi^2 Ra)\delta r_{\rm in} \sim 0.6\,{\rm m}^3$. The density increase on these flux surfaces will depend on the edge ion particle confinement time, which is not directly measured. If we assume that the edge particle confinement time is the same as estimated by UEDGE in section 4.2, i.e. $\tau_{\rm p,edge} \sim 10$ ms, then the estimated rise in edge density averaged over the flux surfaces of the gas cloud is thus $\delta n_{\rm in} = \Gamma_{\rm in}\tau_{\rm p,edge}/V_{\rm edge} \sim 3 \times 10^{13}\,{\rm cm}^{-3}$, where the ionization source is $\Gamma_{\rm in} = 1.8 \times 10^{21}\,{\rm D\,s}^{-1}$ (table 4). This is somewhat smaller than the edge pedestal density at 35 ms after the peak of the puff, but larger than the density at the separatrix, as shown in figure 5.

Next we estimate the maximum *local* edge temperature perturbation expected inside the separatrix due to the energy loss rate of $P_{\rm puff} \sim 10$ kW from radiation and CX from the gas puff (table 4). The perpendicular cross-field heat flux through the gas cloud region for shot #138846 can be roughly estimated by assuming the input power is lost over an area $\sim (2\pi R)\,(\pi a)$ near the outboard midplane, i.e. $P_{\rm edge}/2\pi^2 Ra \sim 4\,{\rm MW}/2 \times 10^5\,{\rm cm}^2 \sim 20\,{\rm W\,cm}^{-2}$. Over the maximum cloud area $\sim$15 cm $\times$ 15 cm $\sim 200\,{\rm cm}^2$ within a flux surface, this perpendicular heat flow is $\sim$5 kW, which is comparable to the radiated power from the gas puff cloud. However, the heat flux coming from upstream along the B should be much larger than the local perpendicular heat flux energy across the gas cloud. Therefore the local radiated power from the gas cloud should create only a small local change in the edge temperature, so it seems reasonable to assume that the edge temperature is nearly constant all along a flux surface through the gas cloud.

With this assumption of constant electron temperature along a flux surface and $T_{\rm i} = T_{\rm e}$, we can estimate the edge energy confinement time and then evaluate the effect of the gas puff radiation on the edge temperature. Within the region between $\rho = 0$–3 cm inside the separatrix, the plasma just before the gas puff has an average $T_{\rm e} = 150$ eV and $n_{\rm e} = 2 \times 10^{13}\,{\rm cm}^{-3}$, so the total stored energy in this volume is $W_{\rm edge} \sim 1$ kJ. The edge energy confinement time is $\tau_{E,\rm edge} \sim W_{\rm edge}/P_{\rm edge}$, where $P_{\rm edge}$ is the power flowing from the main plasma into the edge region. For a shot like #138846, $P_{\rm edge} \sim 4$ MW, thus $\tau_{\rm edge} \sim 1\,{\rm kJ}/4\,{\rm MW} \sim 0.2$ ms. Assuming this $\tau_{\rm edge}$ does not change significantly versus time with the GPI puff, the edge stored energy near the peak of the puff should therefore be $W_{\rm puff} \sim \left(P_{\rm edge} - P_{\rm puff}\right) \times \tau_{E,\rm edge}$, which is very nearly the same as $W_{\rm edge}$ since $P_{\rm puff} \leqslant 10^{-2} P_{\rm edge}$. Thus the stored energy within this region should not decrease significantly due to the puff radiation; however, the electron temperature should decrease by the same fractional amount as the edge density increased during the puff.

We can try to compare these estimates with the measured Thomson scattering data for gas puff shots 138844–138846 within the region $\sim$0–4 cm inside the separatrix (see figure 5). The average measured density increased by $\delta n \sim 0.5 \times 10^{13}\,{\rm cm}^{-3}$ between 35 ms before the peak of the puff and 35 ms after the peak of the puff, or $\sim$15%. The average measured electron temperature decreased by $\sim$15 eV, or $\sim$9% over this same time and space. These are approximately consistent with most of the data in figures 6 and 7 and the statistical fits of table 3, which are mostly $\leqslant$20%. These measured changes are less than the flux-surface averaged effects estimated above, e.g. $\delta n_{\rm in} \sim 3 \times 10^{13}\,{\rm cm}^{-3}$. However, there is significant scatter in the data, and the actual recycling and edge particle confinement time are not known well enough for a good quantitative comparison with the available experimental results. Thus these estimates should only be considered as a first approximation to improved models for the perturbation effects of gas puffs. There are other mechanisms of particle and heat flow into and out of this magnetic flux tube which should be taken into account, such as plasma flows, neoclassical particle drifts, impurity effects and turbulent transport. Very likely 3D models will be needed to calculate the local effects of the gas puff.

4. Discussion

Section 4.1 compares the experimental results and modeling in this paper with previous work, section 4.2 discusses unresolved issues and future directions, and in section 4.3 are the conclusions.

4.1. Relationships to previous experiments and modeling

As mentioned in the Introduction, previous deuterium gas puffing experiments on the PBX-M [5], ADITYA [8, 9] and STOR-M [10] produced significant perturbations in the edge plasma and the edge turbulence. However, gas puffing done for the GPI measurements on Alcator C-Mod [11, 12], EAST [13] and TEXTOR [14] reported no significant perturbations of the gas puff on the edge turbulence, and the present paper basically confirms those results. In general, it is not yet clear what parameter(s) determine the threshold at which a gas puff begins to cause a significant perturbation. This threshold should depend on the gas puff rate, but also on the plasma size, heating power, magnetic geometry, edge particle confinement, edge impurities and radiation, divertor recycling rate, the gas puff location and spatial distribution, and probably other parameters as well. Thus we cannot yet establish a comparative quantitative relationship between the gas puff effects in the present and those in previous experiments.

Most previous modeling of deuterium gas puffing was done to help understand and control divertor plasma detachment. This modeling usually assumed constant gas puffing with simplified edge transport models in codes like UEDGE [35] and SOLPS [53]. The UEDGE modeling of the pulsed gas puff in section 3.2 assumed an axisymmetric gas puff, and so its results could not be directly compared with the localized gas puff and Thomson scattering results of NSTX. Thus this model needs to be further refined and validated for gas puff experiments of this type, e.g. by using a 3D simulation of the gas puff and edge ion transport.

Prior experiments and modeling of deuterium gas puffing was also done in the context of ideas to understand or control the L–H transition [25, 29]. Experimental results previously showed that the L–H transition in NSTX and MAST depended on the location of the gas fueling source [18, 19], which was modeled by the neutral effects on poloidal rotation [27]. However, as described in section 2.6, the gas puffs in the present experiment had no effect on the L–H transition, either to trigger an H-mode from an L-mode plasma or vice versa. This is consistent with the absence of any visible effects of this puff on the edge turbulence or edge plasma velocity in these experiments.

The effects of lithium wall coating on the edge transport and stability have been previously modeled for NSTX using both SOLPS [54] and the microinstability code GS2 [55]. Increased lithium coating can apparently reduce the recycling coefficient and change the edge pressure gradients, which may then affect the edge turbulence and edge transport. The discharges described in this paper had a wide range of lithium coatings (see table 1), with apparently no systematic influence on the deuterium puffing results.

Measurements and modeling of the local effect of a strong gas puff on plasma near the density limit were done in TEXTOR in the radiation increased confinement (RI) regime [16]. At deuterium gas fueling rates up to 9×10^{20} D atom s^{-1} over ~3 s, the local density near the gas puff location increased by up to a factor of ~4 and the local temperature decreased from ~50 to ~10 eV. These changes were fit with a 2-point model, but it is not yet clear how these TEXTOR results with neon seeding near the density limit are related with the present experiments, which were not near the density limit and had no impurity seeding. The latest versions of this model were applied to impurity puffs during massive gas injection [33], and could also be applied to the present experiment.

4.2. Unresolved issues and future directions

The largest unresolved experimental issue in this paper is the effect of the gas puff on the local density and temperature within the gas cloud. The only measurements within the gas cloud were the Dα profiles from the GPI diagnostic, which showed no systematic change with time during the gas puff. It might be possible in the future to infer the local temperatures and densities within the cloud using helium gas mixed into the puff with 2D imaging of the He I line ratios [56, 57]. Local measurements might also be made using a Langmuir probe, and it would be interesting to compare the perturbation due to the probe with that due to the gas puff.

The most surprising experimental result was an occasional decrease in edge electron temperature well after the peak of the puff and inside the radius of its peak ionization, as illustrated in figures 3–5. This decrease occurred on the timescale of ~50–100 ms, i.e. well after the time of peak gas influx rate. This suggests that these perturbation effects may be related to the surface state of the wall or divertor plates, e.g. a higher recycling rate might cause the injected gas to be better retained in the edge. In general, the relationship between wall and divertor recycling and tokamak confinement is still an important and largely unresolved issue.

The deuterium gas puffs used in these experiments did not affect the L–H transition. Further experiments with a higher gas puff influx rate or longer puff duration would help to connect these results to previous measurements which showed such an effect [18, 19]. Future modeling will need to explain the L–H transition in existing discharges and predict its dependence on edge plasma parameters, in order to determine the threshold at which a gas puff will begin to influence the transition in a particular discharge. This modeling should also take into account the X-point geometry and recycling, since these can affect the L–H transition in NSTX even without any explicit consideration of edge turbulence [58].

There are clearly unresolved issues concerning the theory and modeling of the local gas puff effects on the edge plasma. A primary issue is how to calculate the local temperature and density perturbations, given that the heat and particle transport mechanisms in at least two of these three dimensions are not well understood. Progress on this general problem has been made recently and comparisons with massive impurity gas puffing have been made [32, 33]. A comprehensive model for these processes in NSTX should include 3D transport effects, the background edge impurity content and radiation, edge plasma rotation, neoclassical transport, flux surface shaping, and divertor radiation and recycling.

One of the motivations for this paper was to evaluate the possible perturbing effect of the GPI gas puff on the edge turbulence, and the result is that there appears to be no significant perturbing effect. This is not too surprising since even large changes in discharge parameters caused little change in the edge turbulence [42], e.g. varying the NBI power from 2–6 MW in the H-mode shots of figure 12. The edge turbulence in NSTX has only partially been explained by turbulence simulations [59], and in particular the expected sensitivity of the turbulence to neutral gas sources is still unknown, although progress in this area is beginning to be made with the edge turbulence simulation code XGC-1, which is capable of treating the effects of neutrals [60]. A complete model for this experiment should include the specific effects of the 3D localized gas puff on the edge turbulence.

The experimental work on NSTX should be extended to include the analysis of other diagnostic data such as divertor heat flux IRTV measurements, visible imaging of edge and divertor impurity and Dα emission, edge and core impurity content, neutral density measurements, reflectometer edge density and fluctuation profiles, USXR profiles, and ion temperature and rotation profiles. Related experimental work on other devices is also relevant to this future progress; for example, analysis of the gas puff CX diagnostic on Alcator C-Mod [61], the supersonic molecular bean injector on Heliotron J [62], and the effects of helium gas puffing on the divertor asymmetry in EAST [63].

4.3. Conclusions

This paper describes in considerable detail the effects of a small pulsed deuterium gas puff on the edge plasma and edge turbulence in NSTX. This gas puff caused little or no change in the line-averaged plasma density or total stored energy, and the

edge density and electron temperature changed by $\leqslant$10% by time of the peak of the gas puff. However, in some discharges there was a ~20–30% decrease in the electron temperature at ~50–100 ms after the peak of the puff at ~4–10 cm inside the separatrix, the cause of which is not yet understood. The radial profile of the Dα light emission from this gas puff as seen by the gas puff imaging (GPI) diagnostic did not vary significantly over the rise and fall of the gas puff influx rate, which is consistent with nearly constant edge electron temperature and density profiles in the gas cloud ionization region. The edge turbulence seen in the GPI diagnostic (and other edge turbulence diagnostics) did not vary significantly with time during the puff.

Therefore we conclude that the GPI gas puffs used in these NSTX experiments did not significantly perturb either the plasma parameters or the edge turbulence in the region of the Dα emission from these puffs, at least up to the time of the peak of the GPI gas puff influx rate, when most of the previous GPI turbulence measurements have been made. The possible effects at later times should be evaluated on a case-by-case basis.

Modeling of the Dα light emission with DEGAS 2 was consistent with observed GPI images, at least to within the uncertainty of the edge density and temperature profiles as measured by Thomson scattering. Initial UEDGE modeling based on steady-state profiles predicted a factor-of-two increase in edge density and decrease in edge temperature by ~30 ms after the peak of the puff. However, this result was based on an axisymmetric gas puff model, and so could not be directly compared with the localized gas puff and Thomson scattering measurements in NSTX. Therefore further dedicated experiments and 3D modeling are needed to in order understand the response of the edge plasma to localized gas puffs. Future experiments should also be done with a larger range of deuterium gas puff influx rate and duration in order to help clarify the scaling of these effects.

Acknowledgments

The authors would like to thank the NSTX group and particularly D Battaglia, A Diallo, and S Kubota for the gas puffing during their experiments, S Gerhardt, K Tritz, H Schneider and F Scotti for help with diagnostic data and C S Chang, J Lang, R Maingi, and I Shesterikov, L Shao, J L Terry for discussions on this topic. This work was supported by US DOE Contract No. DE-AC02-09CH11466.

References

[1] Sabbagh S A *et al* 2013 *Nucl. Fusion* **53** 014007
[2] Maqueda R J *et al* 2003 *Rev. Sci. Instrum.* **74** 2020
[3] Zweben S *et al* 2004 *Nucl. Fusion* **44** 134
[4] Cao B *et al* 2013 *Fusion Sci. Technol.* **64** 29
[5] Pedrosa M A *et al* 1995 *Phys. Plasmas* **2** 2618
[6] Jacquet P *et al* 2012 *Nucl. Fusion* **52** 042002
[7] Ekedahl A *et al* 2012 *Plasma Phys. Control. Fusion* **54** 074004
[8] Jha R *et al* 2009 *Plasma Phys. Control. Fusion* **51** 095010
[9] Sangwan D, Jha R, Brotankova J and Gopalkrishna M V 2013 *Phys. Plasmas* **20** 062503
[10] Dreval M *et al* 2013 *Plasma Phys. Control. Fusion* **55** 035004
[11] Zweben S J *et al* 2002 *Phys. Plasmas* **9** 1981
[12] Zweben S J *et al* 2013 *Phys. Plasmas* **20** 072503
[13] Liu S C *et al* 2012 *Rev. Sci. Instrum.* **83** 123506
[14] Shesterikov I *et al* 2013 *Rev. Sci. Instrum.* **84** 053501
[15] Panek R *et al* 2005 *J. Nucl. Mater.* **337–339** 530
[16] Unterberg B *et al* 2005 *J. Nucl. Mater.* **337–339** 515
[17] Askinazi L G *et al* 1993 *Phys. Fluids* B **5** 2420
[18] Field A R *et al* 2004 *Plasma Phys. Control. Fusion* **46** 981–1007
[19] Maingi R *et al* 2004 *Plasma Phys. Control. Fusion* **46** A305–13
[20] Strachan J D *et al* 1982 *Nucl. Fusion* **22** 1145
[21] Gentle K W, Richards B and Waelbroeck F 1987 *Plasma Phys. Control. Fusion* **29** 1077
[22] Efthimion P C *et al* 1991 *Phys. Fluids* B **3** 2315
[23] Baker D R *et al* 1998 *Nucl. Fusion* **38** 485
[24] Vershkov V A *et al* 2013 *Nucl. Fusion* **53** 083014
[25] Carreras B A *et al* 1998 *Phys. Plasmas* **5** 2623
[26] Odblom A, Catto P J and Krasheninnikov S I 1999 *Phys. Plasmas* **6** 3239
[27] Helander P, Fulop T and Catto P J 2003 *Phys. Plasmas* **10** 4396
[28] Singh R, Rogister A and Kaw P 2004 *Phys. Plasmas* **11** 129
[29] Miki K *et al* 2013 *Phys. Plasmas* **20** 082304
[30] Tokar M Z 1983 *Nucl. Fusion* **23** 1395
[31] Tokar M Z 1993 *Plasma Phys. Control. Fusion* **35** 119
[32] Tokar M Z and Koltunov M 2013 *Plasma Phys. Control. Fusion* **55** 045013
[33] Tokar M Z and Koltunov M 2013 *Phys. Plasmas* **20** 102502
[34] Petrzilka V *et al* 2012 *Plasma Phys. Control. Fusion* **54** 074005
[35] Porter G D, Petrie T W, Rognlien T D and Rensink M E 2010 *Phys. Plasmas* **17** 112501
[36] Soukhanovskii V A, Kugel H W, Kaita R, Majeski R and Roquemore A L 2004 *Rev. Sci. Instrum.* **75** 4320
[37] Baylor L R *et al* 2013 *Phys. Plasmas* **20** 082513
[38] Maddison G P *et al* 2011 *Nucl. Fusion* **51** 082001
[39] Hollman E H *et al* 2005 *Nucl. Fusion* **45** 1046
[40] Olynyk G M *et al* 2013 *Nucl. Fusion* **53** 092001
[41] Soukhanovskii V A *et al* 2009 *J. Nucl. Mater.* **390–391** 516
[42] Zweben S J *et al* 2009 *Phys. Plasmas* **16** 082505
[43] Tritz K *et al* 2012 *Rev. Sci. Instrum.* **83** 10E109
[44] Biewer T M, Bell R E, Feder R, Johnson D W and Palladino R W 2004 *Rev. Sci. Instrum.* **75** 650
[45] Sechrest Y *et al* 2014 in preparation
[46] Zweben S J *et al* 2010 *Phys. Plasmas* **17** 102502
[47] Sechrest Y, Munsat T, Battaglia D J and Zweben S J 2012 *Nucl. Fusion* **52** 123009
[48] Maqueda R J, Maingi R and the NSTX Team 2009 *Phys. Plasmas* **16** 056117
[49] Soukhanovskii V A *et al* 2003 *J. Nucl. Mater.* **313–316** 573
[50] Stotler D P, Boedo J, LeBlanc B, Maqueda R J and Zweben S J 2007 *J. Nucl. Mater.* **363–365** 686
[51] Rognlien T D, Milovich J L, Rensink M E and Porter G D 1992 *J. Nucl. Mater.* **196** 347–51
[52] Braginskii S I 1965 *Review of Plasma Physics* vol 1, ed M A Leontovitch (New York: Consultants Bureau) pp 205–311
[53] Chen Y P 2011 *Phys. Plasmas* **18** 062506
[54] Canik J M *et al* 2011 *Phys. Plasmas* **18** 056118
[55] Canik J M *et al* 2013 *Nucl. Fusion* **53** 113016
[56] Agostini M *et al* 2010 *Rev. Sci. Instrum.* **81** 10D715
[57] de la Cal E, Guasp J and the TJ-II Team 2011 *Plasma Phys. Control. Fusion* **53** 085006
[58] Battaglia D J *et al* 2013 *Nucl. Fusion* **53** 113032
[59] Myra J R *et al* 2013 *Nucl. Fusion* **53** 073013
[60] Lang J and Chang C S 2014 private communication
[61] Theiler C *et al* 2014 *Nucl. Fusion* **54** 083017
[62] Zang L *et al* 2014 *Phys. Plasmas* **21** 042308
[63] Liu S C *et al* 2014 *Phys. Plasmas* **21** 022509